Science Immunology
AAAS

immunology.sciencemag.org/cgi/content/full/4/32/eaal2201/DC1

# Supplementary Materials for

## The early proximal αβ TCR signalosome specifies thymic selection outcome through a quantitative protein interaction network

Steven C. Neier, Alejandro Ferrer, Katelynn M. Wilton, Stephen E. P. Smith, April M. H. Kelcher, Kevin D. Pavelko, Jenna M. Canfield, Tessa R. Davis, Robert J. Stiles, Zhenjun Chen, James McCluskey, Scott R. Burrows, Jamie Rossjohn, Deanne M. Hebrink, Eva M. Carmona, Andrew H. Limper, Dietmar J. Kappes, Peter J. Wettstein, Aaron J. Johnson, Larry R. Pease, Mark A. Daniels, Claudia Neuhauser, Diana Gil*, Adam G. Schrum*

*Corresponding author. Email: schruma@health.missouri.edu (A.G.S.); gilpagesd@health.missouri.edu (D.G.)

Published 15 February 2019, *Sci. Immunol.* **4**, eaal2201 (2019)
DOI: 10.1126/sciimmunol.aal2201

**The PDF file includes:**

**Other Supplementary Material for this manuscript includes the following:**

(available at immunology.sciencemag.org/cgi/content/full/4/32/eaal2201/DC1)

Table S2 (Microsoft Excel format). Raw data for experiments with $n \leq 25$.

## Results and Discussion

### PiSCES can distinguish qualitative from quantitative signaling activities in primary pre-selection thymocytes

We validated that the PiSCES system was capable of detecting qualitatively distinct PPI network activity from primary OT1.RAG2$^0$.b2m$^0$ pre-selection thymocytes, by comparing two commonly employed non-physiologic stimuli, pervanadate (PV) and $H_2O_2$. A known difference between these two stimuli can be considered somewhat analogous to that reported for agonist versus antagonist pMHC stimuli (*10, 56-58*), since PV generates fully phosphorylated immunoreceptor tyrosine-based activation motifs (ITAM) in CD3ζ, while $H_2O_2$ generates partial ITAM phosphorylation only (*75*).

While comparing PV to $H_2O_2$ stimuli, high (strong) or low (weak) concentrations of either stimulatory agent were also administered in order to analyze PiSCES networks that would represent pre-defined quantitative dose differences.We began by analyzing the pre-defined quantitative-only differences observed with either stimulatory agent, starting with $H_2O_2$ (Fig. S2A-F). When protein pair hits from the strong dose of $H_2O_2$ were normalized to matched measurements from the weak dose, most hits were observed in the positive direction (red, Fig. S2A), meaning that protein pair measurements increased with stronger stimulation. Some hits, however, were observed in the negative direction (blue, Fig. S2A). Comparing hits observed in the strong versus weak stimulus conditions, the absolute value of the responses to strong stimulation were usually greater than the absolute value of responses to the weak stimulation (purple points, Fig. S2B). This indicated that the magnitude of fold-change for each protein pair

tended to be greatest in the stronger stimulus, regardless of whether that change was in the positive or negative direction. This observation was corroborated by examining the data another way, by separating all hits observed in the strong/weak comparison (Fig. S2A) based on the direction of their change, and examining each hit separately in strong/null (Fig. S2C,E) or weak/null (Fig. S2D,F) visualizations. In basic terms, the data in Supplementary Fig. 2C appeared redder than those in Supplementary Fig. 2D, and the data in in Supplementary Fig. 2E were bluer than those in Supplementary Fig. 2F.This meant that all strong/weak positive hits were highest for the strong stimulus (strong/null, Fig. S2C compared with weak/null, Fig. S2D), while negative hits were more negative for the strong stimulus (strong/null, Fig. S2E compared with weak/null, Fig. S2F). A similar pattern could also be attributed to most hits observed when PV was used in strong versus weak concentrations to stimulate thymocytes (Fig. S3A-F). We conclude that in pre-defined stimuli whose differences are quantitative-only, an absolute-value effect can be observed, in which the magnitude of fold-change for each protein pair is greatest in response to the stronger stimulus, regardless of whether that change is in the positive or negative direction.

In contrast, comparing strong PV to strong $H_2O_2$, it was clear that these two stimuli were not simply dilutions of each other, as each induced a different balance of activity in its PiSCES signature. Normalizing PV to $H_2O_2$ data, we found that hits of induced protein pairs were observed in favor of either stimulus (Fig. S2G:red, higher in PV; blue, higher in $H_2O_2$). However, unlike pre-defined quantitative stimulus dilutions (Fig. S2B), plotting the protein pair inductions for both stimuli revealed many hits that were of relatively greater magnitude in PV than $H_2O_2$, and additionally a substantial number of hits that were greater in $H_2O_2$ than PV (Fig.

S2H). When examining PV/$H_2O_2$ hits individually in PV/null and $H_2O_2$/null conditions, it was observed that hits that were higher in PV/$H_2O_2$ could be so whether their change occurred in the positive or negative direction (Fig. S2I-J), and the same was true for other hits that were higher in $H_2O_2$ (Fig. S2K-L). Together, these data showed that PV and $H_2O_2$ stimuli did not produce the same network PPI activity whose only difference could be accounted for by a quantitative-only change across the signature. We conclude that, in contrast to positive versus negative selection stimuli, non-physiologic stimuli made it possible to impose upon pre-selection DP thymocytes the transduction of qualitatively unique network signatures through the proximal TCR signalosome.

**Expression of CD8αα in FTOC cells**

A unique developmental sequence has been delineated for physiologic CD8αα SP T cells (reviewed in (*76*)).They originate from triple-positive thymocytes expressing CD4, CD8αβ, and CD8αα, and upon selection they downregulate these receptors to rejoin the DN thymocyte pool before thymic export. It is upon migration to mucosal tissues that they re-upregulate CD8αα. Because the CD8α+ CD8β- SP T cells that developed in the present FTOC experiments did so while residing in thymic tissue, the extent to which these cells might be representative of physiologic CD8αα SP T cells is not clear. As in Figure 4, FTOCs using OT1.RAG2$^0$.β2m$^0$thymi and exogenous β2m plus peptides were performed to analyze CD8αα expression using tetramers of the ligand, Thymic Leukemia Antigen (TLA). First, we observed that across all FTOC conditions most CD8β+ cells were also TLA+ (Fig. S9A-D, upper right gates), which is similar to data reported for fresh harvests of fetal thymi at embryonic day (e)17,

but not adjacent days e16 or e18 (Ref. (*77*)). We wished to determine whether the known pattern of change in CD8αα expression during the development of physiologic CD8αα SP T cells would be predictive of patterns observed in the present FTOCs. Therefore, we considered 3 populations as relevant to CD8αα SP developmental progression:CD8β+ TLA+ (predicted originator subset), CD8β- TLA- (predicted post-selection thymic product), CD8β- TLA+ (predicted post-thymus product, but possibly observed prematurely in FTOC).The relative distribution of cells in these 3 subsets appeared to be similar when comparing conditions of no-selection (FARL 0.75 nM) and conventional positive selection (Q7 20 μM, and OVA 0.75 nM) (Fig. S9A-C).In contrast, the relative frequency of both potential product subsets, CD8β- TLA- and CD8β- TLA+ (CD8αα+), were significantly increased in the putative CD8αα SP-generating condition (OVA 3 nM) (Fig. S9D-G). We conclude that selection in FTOC of T cells that appear to differentiate along a CD8αα SP pathway shares a feature in common with physiologic CD8αα SP T cell selection, in that both require stronger signals ("agonist-selection") than those that generate conventional CD8αβ SP T cells.

**Development of proliferative and cytotoxic T lymphocyte (CTL) capability in response to antigenic stimulation by OT1 cells from positive selection FTOC conditions**

To determine whether the OVA 0.75 nM FTOC condition could generate functional T cells, we performed experiments modeled after a proliferation-assay strategy previously published by Hogquist et al. (*27*). FTOC was performed using conditions favoring conventional positive selection (Q7 20 μM), unconventional selection (OVA 3nM), negative selection (OVA 20 μM), or the putative conventional positive selection condition, OVA 0.75 nM.Following FTOC,

single-cell suspensions of FTOC cells were co-cultured with CD3$\varepsilon^0\zeta^0$splenocyte APCs that had been previously pulsed with 10 nM FARL or OVA peptides, a concentration that was chosen based on its reported optimization for stimulation of OT1 cells developed in FTOC (*27*).After 3 days of co-culture, exogenous mouse IL-2 was added and incubation continued up to 12 total days. We observed that low T cell numbers decreased over time in most experimental groups, but T cell numbers increased in co-cultures presenting OVA to post-FTOC cells from Q7 20 μM and OVA 0.75 nM conditions (Fig. S10A). We wished to determine if these cells had developed CTL capability. On day 12 post-co-culture, expanded post-FTOC cells originating from Q7 20 μM or OVA 0.75 nM conditions were co-cultured with a new set of CD3$\varepsilon^0\zeta^0$splenocyte APCs as targets, this time loaded with 10 μM FARL or OVA peptides. We found that both sets of post-FTOC T cells possessed specific cytotoxic activity against OVA-directed targets when compared to non-specific CTL activity of B6 splenocytes (Fig. S10B). Because these conditions showed limited (but significant) proliferation and killing, we sought to use a system that might favor post-FTOC T cell maturation and capacitation, *in vivo* (Ref. (*78*); Fig. S10C-H). Single-cell suspensions from Q7 20 μM or OVA 0.75 nM FTOC conditions were adoptively transferred into $Rag2^0$.$IL2Rg^0$ recipients. After 40 days, mice that either had or had not received adoptive transfers were infected with TMEV-OVA8 virus, a genetically engineered Theiler's Murine Encephalomyelitis Virus that expresses SIINFEKL from ovalbumin (*79*). This viral immunization system was chosen because it is known to induce T cell responses that do not require CD4 T cell help (*80*). Three days after infection, an *in vivo*-CTL assay was begun by injecting mice with Ly5.1+ congenic splenocyte APCs that were composed of an equal mixture of FARL-loaded (CFSE-low) and OVA-loaded (CFSE-high) cells. Finally, one day later, upon harvest of host splenocytes, we observed that mice that had received post-FTOC cells from either

Q7 20 μM or OVA 0.75 nM conditions showed high and comparable capacity for specific lysis of OVA-bearing APCs (Fig. S10G-H). We conclude that cells from the OVA 0.75 nMFTOC condition were not non-functional, and were able to display similar immune functional potential when compared to the positive control for positive selection, Q7 peptide.

## Materials and Methods

### T cell stimulation by Pervandadate (PV) or $H_2O_2$

15 x $10^6$ pre-selection OT1.β2m$^0$.RAG2$^0$ DP thymocytes were stimulated in 200 μL PBS plus either PV, $H_2O_2$, or PBS no-stimulation control for 5 minutes at 37ºC, followed by 2 minute centrifugation at 300g and flash-freezing in liquid nitrogen. The high (strong) dose of PV was 40 μM sodium orthovanadate + 1.25 mM $H_2O_2$, while the low (weak) dose was 8 μM sodium orthovanadate + 0.25 mM $H_2O_2$. The high (strong) dose of $H_2O_2$ was 8.85 mM, while the low (weak) dose was 1.75 mM. Lysis, multiplex IP, and other experimental procedures were performed as described in the main text.

### FTOC-generated T cell response to antigenic stimulation, *in vitro*

OT1.Rag2$^0$.β2m$^0$ fetal thymi were subjected to FTOC as described using the following peptide conditions:Q7, 20 μM; OVA, 0.75 nM; OVA, 3nM; OVA, 20 μM.Splenocyte APCs from CD3ε$^0$ζ$^0$ mice were cultured for 2 hours, 37˚C, in the presence of 10 nM FARL or OVA peptides. Post-FTOC cells in single-cell suspension were mixed with APCs at 1:1 ratio. After 72 hours of incubation, ¼ volume was added of supernatant from X63Ag8-653.IL2 cells (~100 U/mL final volume of mouse IL-2, Ref. (*81*)). Live T cells were counted by multiplying total live cell counts by percent Thy1.2+ assessed by flow cytometry on days 4, 8, and 12. To test post-co-culture FTOC-generated cells for CTL potential, target cells were prepared using new splenocyte APCs from CD3ε$^0$ζ$^0$ mice that were loaded with 10 μM FARL or OVA peptides for 2 hours at 37˚C. Target cells were labeled with two different concentrations of CFSE (FARL, low CFSE; OVA, high CFSE). Post-co-culture cells were then mixed with FARL- and OVA-loaded target

cells at 20:1:1 ratio, and incubated for 24 hours, 37˚C. Samples were harvested and stained with anti-Thy1.2 and propidium iodide (PI) and analyzed using an Accuri C6 flow cytometer (BD). Live target cell counts for FARL (CFSE low) and OVA (CFSE high) were obtained by gating on live (PI–), Thy1.2-negative populations. Specific lysis was calculated using the following formula: %Specific Lysis = 1 – [ $r_{\text{Target cultures, no CTL}}$ / $r_{\text{ Target \& CTL co-cultures}}$] X 100. Where $r$ = CFSE-low cell number / CFSE-high cell number.

**FTOC-generated T cell response to antigenic stimulation, *in vivo***

OT1.Rag2$^0$.β2m$^0$ fetal thymi were subjected to FTOC in the presence of either Q7 20 μM or OVA 0.75 nM, as described. Single-cell suspensions were injected retro-orbitally into RAG2$^0$.IL2Rg$^0$ recipient mice. Forty days later, mice were infected i.p. with 2x10$^5$ PFU of TMEV-OVA8 virus as described (*79*). Three days afterward, CFSE-labeled Ly5.1+ congenic splenocyte APCs that had been loaded with FARL (CFSE-low) or OVA (CFSE-high) were mixed in equal proportions and injected intravenously. Finally, 24 hours later, spleens were harvested, and single-cell suspensions were prepared for flow cytometry by staining, first with H-2Kb-SIINFEKL (OVA)-tetramer for 30-60 minutes at 25-37ºC to permit tetramer internalization. Second, without washing, additional staining reagents were added and incubated for 30 minutes, including anti-Ly5.1 to detect target cells, and anti-CD8β. Cells were washed and analyzed by flow cytometry. Relative cell proportions for both FARL- and OVA-loaded target cells were obtained by gating on live, Ly5.1+ cells and analyzing CFSE-low and CFSE-high populations.Specific lysis was calculated using the formula: %Specific Lysis = 1 – [ $r_{\text{no FTOC transfer}}$ / $r_{\text{FTOC-transfer}}$ ] X 100. Where $r$ = $\text{CFSE}_{\text{low}}$ cell number / $\text{CFSE}_{\text{high}}$ cell number.

**Quantification of T cell percentage in peripheral blood**

Peripheral blood from OT1.Rag2$^0$, OT1.Rag2$^0$.CD3δ$^0$, and OT1.Rag2$^0$.β2m$^0$.CD3δ$^0$ mice was collected in EDTA-coated tubes.Leukocytes were isolated using Ficoll gradient centrifugation and incubated for 30 min on ice with antibody stains.Flow cytometry was performed using an Accuri C6 apparatus (BD) and results were analyzed using FlowJo software (Treestar, Inc.).

**Details of TCR BVJ Repertoire Analysis**

Total RNA was extracted from up to 5 x 10$^6$splenocytes from individual mice using an RNeasy Protect MiniKit (Qiagen, Valencia, CA) according to the manufacturer's instructions. Up to 15 ng of total RNA was delivered to each of four RT-PCRs that were performed with a reverse BC region primer that was biotinylated at the 5' end and four pools of BV-specific primers (three pools of five primers and one pool of six primers) that were homologous to the CDR1 regions of their respective BV genes.The primer sequences have been previously described (*49*), and all primers were synthesized by the Invitrogen Supply Center located in the Mayo Clinic Primer Core Facility.cDNA was synthesized at 50°C for 32 min followed by incubation at 95°C for 15 min to inactivate the reverse transcriptase.Subsequent PCR parameters were 60 sec at 94°C, 30 sec at 60°C, and 60 sec at 72°C for 25 cycles.A final extension cycle was performed for 6 min at 72°C.RT-PCR products were separated from residual primers and amplification reagents using a QIAquick PCR Purification Kit (Qiagen), and biotinylated RT-PCR products were enriched with magnetic My One$^{TM}$ Streptavidin C1 Dynabeads (Dynal Biotech ASA, Oslo, Norway) using the manufacturer's protocol.

A total of 252 individual real-time PCRs (21 BV and 12 BJ primers) were performed in 10 μL volumes in 384-well Clear Optical Reaction Plates with Optical Adhesive Covers (Applied Biosystems).The components of reactions were (i) the respective RT-PCR product-bound bead suspension, (ii) Power SYBR Green PCR Master Mix (Applied Biosystems), (iii) a nested BV primer, and (iv) a BJ-specific primer.Cycling was performed on an ABI Prism 7900HT Sequence Detection System at the AGTC Microarray Shared Resource Core Facility (Mayo Clinic) using SYBR Green detection.Cycling parameters were as follows: an incubation at 50°C for 2 min, a 10 min incubation at 95°C to activate the DNA polymerase, and 40 cycles of 15 sec at 95°C followed by 60 sec at 60°C.Dissociation curves were generated by incubating the amplicons at 95°C for 15 sec, reducing the temperature to 60°C for 15 sec, and increasing the temperature to 95°C over a dissociation time of 20 min.Data were analyzed with the 7900HT Sequence Detection System (SDS) Version 2.3 software (Applied Biosystems) to estimate cycle threshold (Ct) values and dissociation curves to estimate the optimal melting temperatures for all reactions.Ct values were automatically set to be within the exponential region of the amplification curve where there was a linear relationship between the log of change in fluorescence and cycle number.Rising temperatures versus the change in fluorescence/change in temperature were plotted to generate dissociation curves.

*Estimates of Diversity*.The relative abundance of individual BV:BJ combinations was definedby the observed Ct values. Dissociation curves were used toconfirm the presence of amplicons from beta transcripts byexcluding (i) primer-dimers that had relatively low melting temperatures and

(ii) amplicons with dissociation peak heightsthat did not exceed a threshold of 0.07 (change in fluorescence/changein temperature).This threshold was selected experimentallydue to the inability to sequence amplicons that were below thisvalue. Amplicons with either or both of these characteristicswere assigned Ct values of 40 cycles. The diversities ofthe 252 BV:BJ combinations within individual RNA templateswere estimated by Shannon entropy, a value that has been used forestimating variability at individual amino acid positions inimmunoglobulin and TcR V gene products (*49, 82*). An estimateof scaled entropy (H) was calculated for each BV:BJ matrixby the equation $H = \sum(P \log_2 P)/\log_2(1/252)$ where $P$ was the probabilityof abundance calculated for each BV:BJ combination bythe equation $P = 2^{-y}/\sum 2^{-y}$ where $y$ was the Ct valuefor the BV:BJ primer pair and $P = 0$ when Ct = 40 cycles.

For data shown in Fig. 7 (and Fig.S14), 15 ng RNA was used per mouse of each genotype, and therefore the contribution of T cells to total RNA was greater for B6 (T cell sufficient) than for CD3$\delta^0$ (T cell deficient). First, we wished to visualize the highest potential of a mouse from either genotype to generate RNA for TCRβ, while allowing the natural difference in T cell number to be a factor when assessing transcript quantities. Therefore, the maximal generation potential of TCR RNA of B6 and CD3$\delta^0$ per mouse was visualized by selecting for data representation the individual (Fig. S14) or average Ct values from the top two individuals (Fig. 7) with highest entropy from each genotype (top 2 of four B6, top 2 of six CD3$\delta^0$ mice tested). (Note:this analysis does not include average Ct values from all mice tested, for a specific reason that we feel is most compatible with our use of entropy as an estimate of diversity. Recall that entropy is highest (approaches 1) when all transcripts are expressed at equal levels. Taking the average Ct values from all mice removes much of the natural variability, producing a flattening

or evening effect on the data that can inflate both the entropy calculation and the "impression" of evenness of expression in visualizations. Therefore, we limited entropy calculations to data from individual mice only, and we did not visualize average Ct values from all mice of either genotype.) In contrast, to assess diversity when both genotypes provided input RNA from comparable numbers of T cells, splenocyte RNA from each of two B6 mice was reduced to approximate the T cell contribution present in 15 ng RNA from CD3$\delta^0$ mice (discussed in Results subsection, *The $\alpha\beta$ TCR repertoire in peripheral CD3$\delta^0$ T cells is diverse).*

**TCRαSpectratyping**

TCRαspectratype analysis was performed with primer sequences and protocols as previously described in detail (*50, 51*).

**Supplementary Figures & Legends**

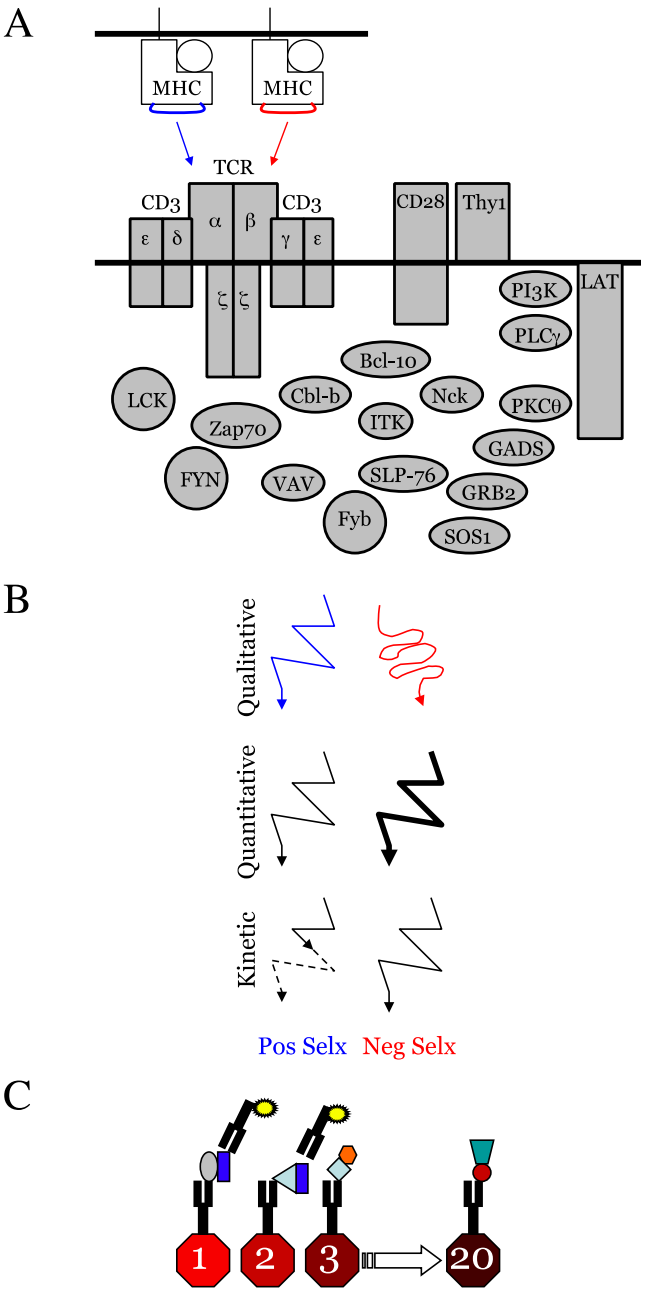


**Fig. S1. Theoretical framework to categorize network patterns of TCR-proximal signaling protein complexes that could specify positive versus negative selection. (A)** Upon engagement of TCR by a selection pMHC ligand, signal transduction occurs through a well-studied cascade of proteins that bind each other through protein-protein interactions to form

signaling complexes.Approximately 20 of these proteins are shown here (although some multimeric complexes are counted as a single unit, such as heteromeric TCR/CD3 or homodimeric CD28, for example). **(B)** The network mechanism by which the proximal TCR signalosome specifies positive versus negative selection outcome through signaling protein complexes is incompletely understood. Signal specificity might be instructed by qualitatively distinct sets of protein complexes that transduce different signals, or by quantitative or kinetic differences in protein complexes. The present experiments are designed to distinguish between these possibilities. **(C)** Multiplex immunoprecipitation from lysates is performed when protein complexes are immune precipitated on microsphere color-classes coupled to capture antibodies, and the captured complexes are probed with fluorophore-coupled detection antibodies for flow cytometry analysis.

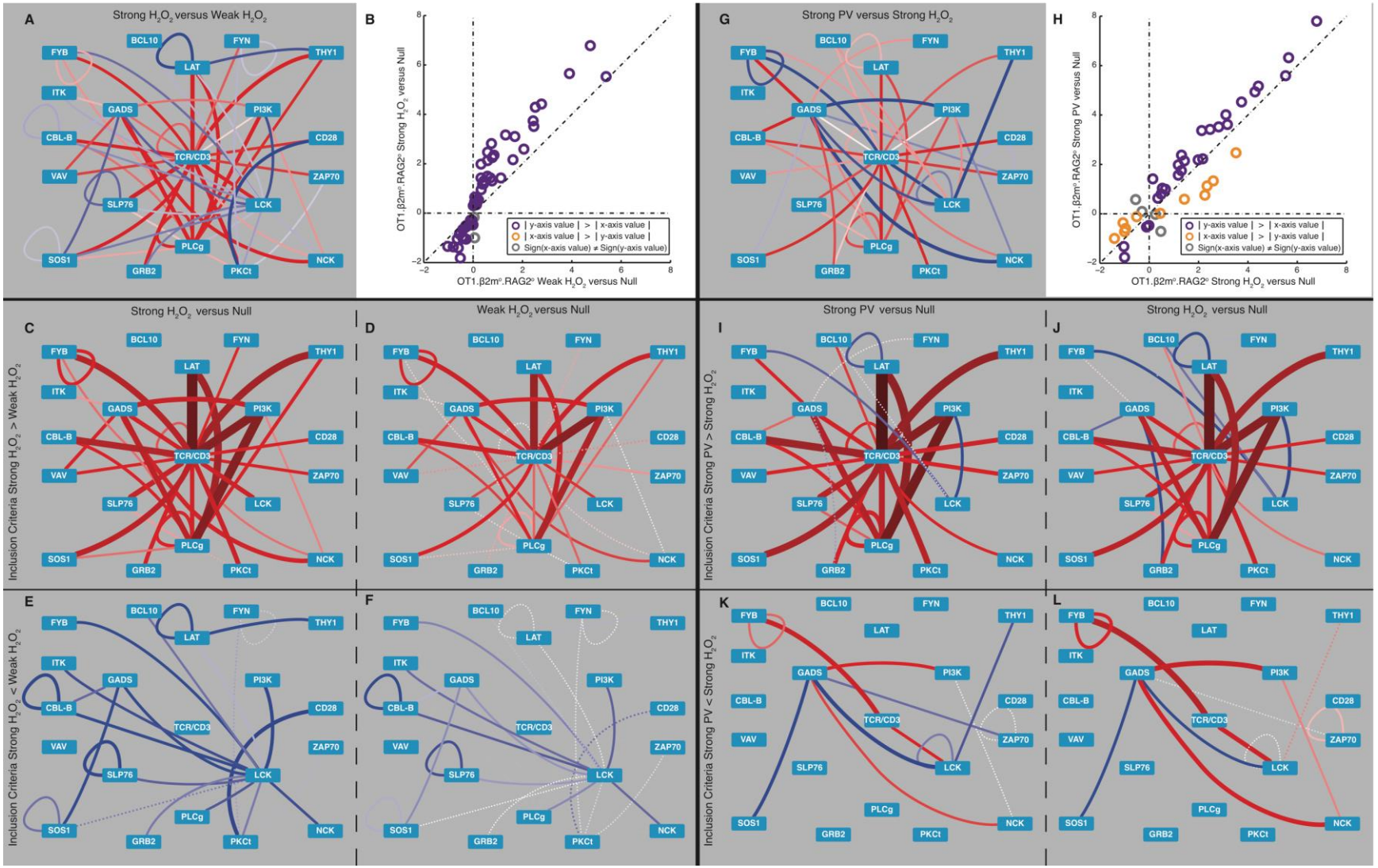
A
Strong H2O2 versus Weak H2O2
B
OT1.β2m-.RAG2- Strong H2O2 versus Null
OT1.β2m-.RAG2- Weak H2O2 versus Null
| y-axis value | > | x-axis value |
| x-axis value | > | y-axis value |
Sign(x-axis value) ≠ Sign(y-axis value)
G
Strong PV versus Strong H2O2
H
OT1.β2m-.RAG2- Strong PV versus Null
OT1.β2m-.RAG2- Strong H2O2 versus Null
C
Strong H2O2 versus Null
Inclusion Criteria Strong H2O2 > Weak H2O2
D
Weak H2O2 versus Null
I
Strong PV versus Null
Inclusion Criteria Strong PV > Strong H2O2
J
Strong H2O2 versus Null
E
Inclusion Criteria Strong H2O2 < Weak H2O2
F
K
Inclusion Criteria Strong PV < Strong H2O2
L
BCL10
FYN
THY1
LAT
FYB
ITK
GADS
PI3K
CBL-B
CD28
TCR/CD3
VAV
ZAP70
SLP76
LCK
PLCg
SOS1
GRB2
PKCt
NCK

**Fig. S2. The response of preselection OT1.β2m$^0$.RAG2$^0$ DP thymocytes to $H_2O_2$, and comparison with PV stimulation. (A-F)** Comparing the response to high-dose (strong) versus low-dose (weak) $H_2O_2$ stimulation. **(A)** PiSCES signature of OT1.β2m$^0$.RAG2$^0$thymocytes stimulated with high-dose (strong) or low-dose (weak) $H_2O_2$ for 5 minutes (mean-log2 fold-change, strong/weak; dotted lines indicate trend of non-significant protein pairs that appear as hits in other comparator graphs in this figure). **(B)** Comparison of mean-log2 fold-changes in abundance of protein pair hits induced by high-dose (strong) versus low-dose (weak) $H_2O_2$. **(C-F)** Protein pair hits are only plotted if they were statistically significant in the strong/weak comparison shown in panel (A). **(C)**PiSCES signature of OT1.β2m$^0$.RAG2$^0$thymocytes stimulated with high-dose (strong) for 5 minutes (mean-log2 fold-change, strong/null), plotting protein pair hits that were higher in the strong versus the weak stimulus condition. **(D)**PiSCES signature of OT1.β2m$^0$.RAG2$^0$thymocytes stimulated with low-dose (weak) for 5 minutes (mean-log2 fold-change, weak/null), plotting protein pair hits that were higher in the strong versus the weak stimulus condition. **(E)**PiSCES signature of OT1.β2m$^0$.RAG2$^0$thymocytes stimulated with high-dose (strong) for 5 minutes (mean-log2 fold-change, strong/null), plotting protein pair hits that were lower in the strong versus the weak stimulus condition.**(F)**PiSCES signature of OT1.β2m$^0$.RAG2$^0$thymocytes stimulated with low-dose (weak) for 5 minutes (mean-log2 fold-change, weak/null), plotting protein pair hits that were lower in the strong versus the weak stimulus condition. **(G-L)**Comparing the response to high-dose (strong) PV versus high-dose (strong) $H_2O_2$ stimulation.**(G)** PiSCES signature of OT1.β2m$^0$.RAG2$^0$thymocytes stimulated with PV or $H_2O_2$ for 5 minutes (mean-log2 fold-change, PV/$H_2O_2$; dotted lines indicate trend of non-significant protein pairs that appear as hits

in other comparator graphs in this figure). **(H)** Comparison of mean-log2 fold-changes in abundance of protein pair hits induced by PV versus $H_2O_2$. **(I-L)** Protein pair hits are only plotted if they were statistically significant in the PV/$H_2O_2$ comparison shown in panel (G). **(I)**PiSCES signature of OT1.β2m$^0$.RAG2$^0$thymocytes stimulated with PV for 5 minutes (mean-log2 fold-change, PV/null), plotting protein pair hits that were higher in PV versus $H_2O_2$ stimulus condition. **(J)**PiSCES signature of OT1.β2m$^0$.RAG2$^0$thymocytes stimulated with $H_2O_2$ for 5 minutes (mean-log2 fold-change, $H_2O_2$/null), plotting protein pair hits that were higher in PV versus $H_2O_2$ stimulus condition. **(K)**PiSCES signature of OT1.β2m$^0$.RAG2$^0$thymocytes stimulated with PV for 5 minutes (mean-log2 fold-change, PV/null), plotting protein pair hits that were lower in the PV versus $H_2O_2$ stimulus condition.**(L)**PiSCES signature of OT1.β2m$^0$.RAG2$^0$thymocytes stimulated with $H_2O_2$ for 5 minutes (mean-log2 fold-change, $H_2O_2$/null), plotting protein pair hits that were lower in PV versus $H_2O_2$ stimulus condition.

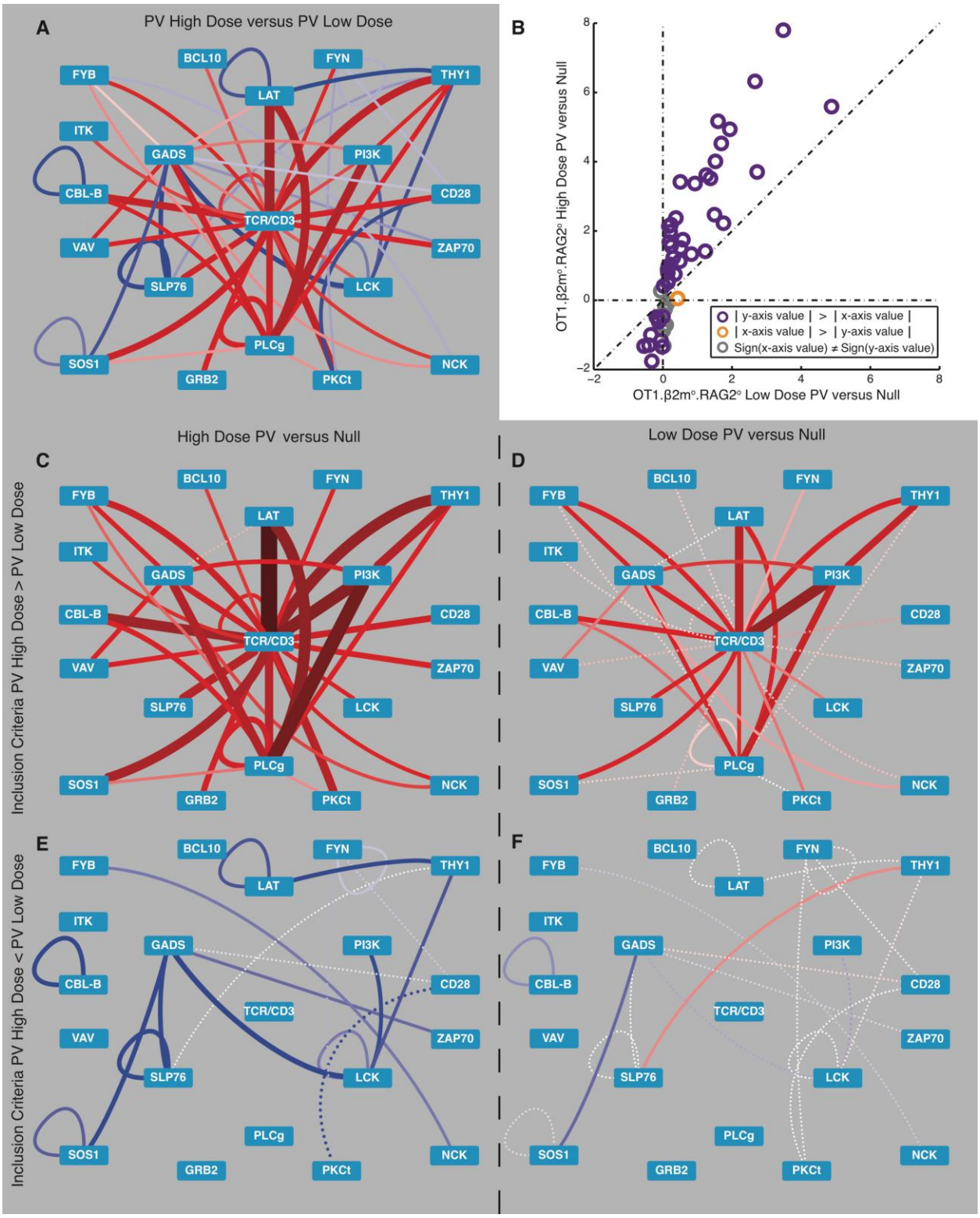
A
PV High Dose versus PV Low Dose
BCL10
FYN
FYB
THY1
LAT
ITK
GADS
PI3K
CBL-B
CD28
TCR/CD3
VAV
ZAP70
SLP76
LCK
PLCg
SOS1
NCK
GRB2
PKCt
B
OT1.β2m°.RAG2° High Dose PV versus Null
OT1.β2m°.RAG2° Low Dose PV versus Null
| y-axis value | > | x-axis value |
| x-axis value | > | y-axis value |
Sign(x-axis value) ≠ Sign(y-axis value)
C
High Dose PV versus Null
D
Low Dose PV versus Null
Inclusion Criteria PV High Dose > PV Low Dose
E
F
Inclusion Criteria PV High Dose < PV Low Dose

**Fig. S3. The response of preselection OT1.β2m$^0$.RAG2$^0$ DP thymocytes to PV stimulation.** **(A-F)** Comparing the response to high-dose (strong) versus low-dose (weak) PV stimulation.**(A)** PiSCES signature of OT1.β2m$^0$.RAG2$^0$thymocytes stimulated with high-dose (strong) or low-dose (weak) PV for 5 minutes (mean-log2 fold-change, strong/weak; dotted lines indicate trend of non-significant protein pairs that appear as hits in other comparator graphs in this figure). **(B)** Comparison of mean-log2 fold-changes in abundance of protein pair hits induced by high-dose (strong) versus low-dose (weak) PV. **(C-F)** Protein pair hits are only plotted if they were statistically significant in the strong/weak comparison shown in panel (A). **(C)**PiSCES signature of OT1.β2m$^0$.RAG2$^0$thymocytes stimulated with high-dose (strong) for 5 minutes (mean-log2 fold-change, strong/null), plotting protein pair hits that were higher in the strong versus the weak stimulus condition. **(D)**PiSCES signature of OT1.β2m$^0$.RAG2$^0$thymocytesstimulated with low-dose (weak) for 5 minutes (mean-log2 fold-change, weak/null), plotting protein pair hits that were higher in the strong versus the weak stimulus condition. **(E)**PiSCES signature of OT1.β2m$^0$.RAG2$^0$thymocytes stimulated with high-dose (strong) for 5 minutes (mean-log2 fold-change, strong/null), plotting protein pair hits that were lower in the strong versus the weak stimulus condition.**(F)**PiSCES signature of OT1.β2m$^0$.RAG2$^0$thymocytes stimulated with low-dose (weak) for 5 minutes (mean-log2 fold-change, weak/null), plotting protein pair hits that were lower in the strong versus the weak stimulus condition

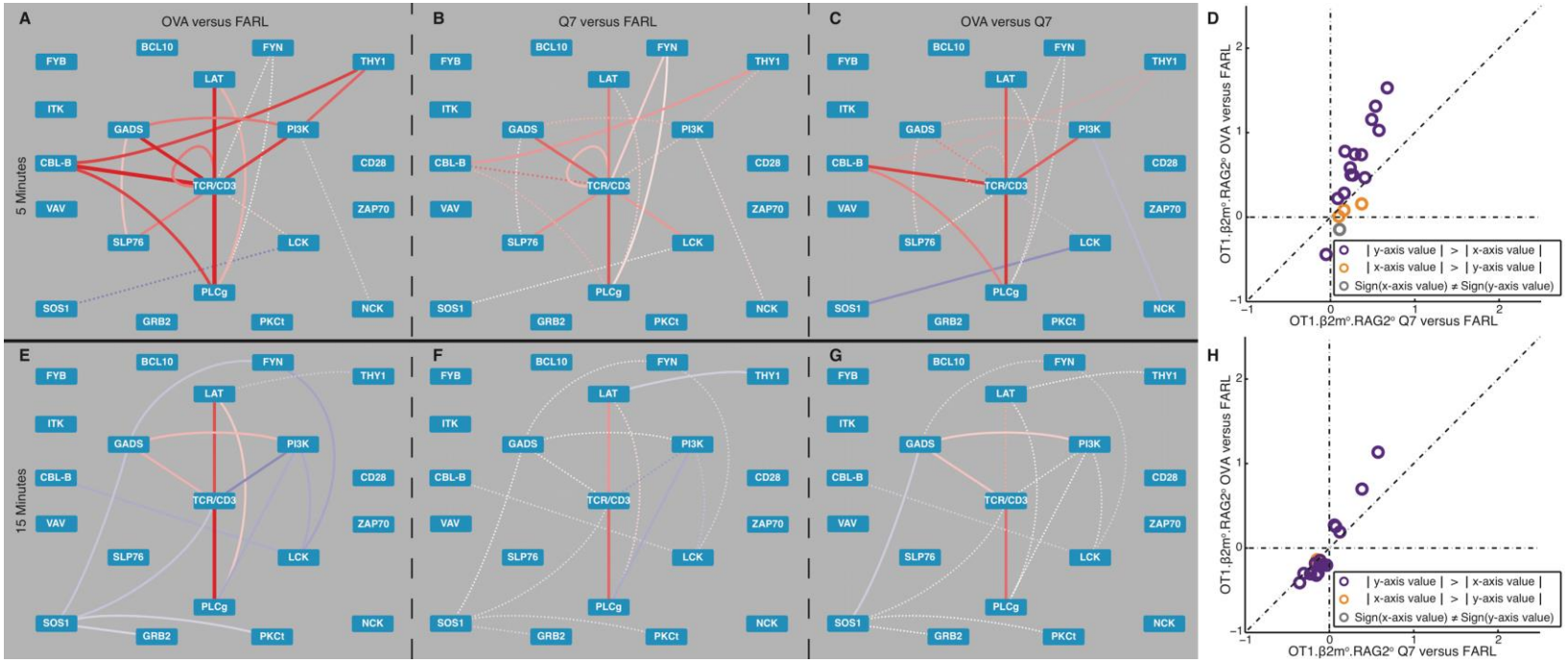


**Fig. S4. Kinetics of PiSCES signatures for positive and negative selection stimuli.** PiSCES signatures of pre-selection OT1.β2m$^0$.RAG2$^0$thymocytes stimulated for **(A-D)** 5 minutes, or **(E-H)** 15 minutes with **(A,E)** negative selection peptide, OVA (mean-log2 fold-change, OVA/FARL conditions; dotted lines indicate trend of non-significant protein pairs across a given time point), or **(B,F)** positive selection peptide, Q7 (mean-log2 fold-change, Q7/FARL conditions). **(C,G)** PiSCES signatures when response to OVA is directly normalized to the response to Q7 (mean-log2 fold-change, OVA/Q7 conditions). **(D,H)** Comparisons of mean-log2 fold-changes in abundance of protein pair hits induced by OVA versus Q7 in pre-selection OT1.β2m$^0$.RAG2$^0$thymocytes.Data points are displayed for hits that were statistically significant in any of the OVA versus FARL, Q7 versus FARL, or OVA versus Q7 comparisons. A separate trajectory of orange points (|*x*-axis value| > |*y*-axis value|) that would clearly indicate positive selection-specific protein complexes is not observed.

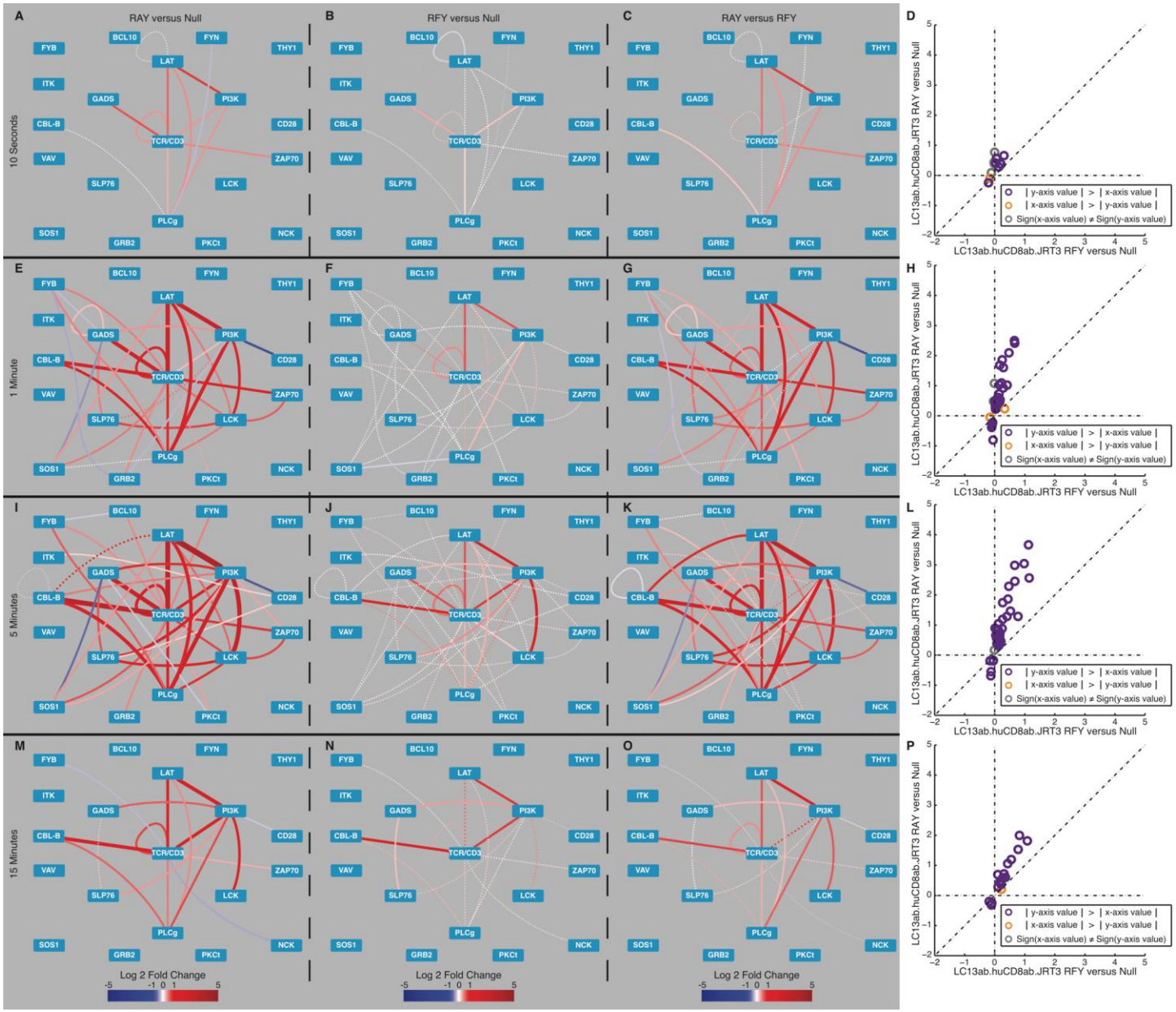
A
RAY versus Null
B
RFY versus Null
C
RAY versus RFY
D
10 Seconds
E
F
G
H
1 Minute
I
J
K
L
5 Minutes
M
N
O
P
15 Minutes
BCL10
FYN
THY1
FYB
LAT
ITK
GADS
PI3K
CBL-B
CD28
TCR/CD3
VAV
ZAP70
SLP76
LCK
PLCg
SOS1
GRB2
PKCt
NCK
Log 2 Fold Change
-5 -1 0 1 5
LC13ab.huCD8ab.JRT3 RAY versus Null
LC13ab.huCD8ab.JRT3 RFY versus Null
| y-axis value | > | x-axis value |
| x-axis value | > | y-axis value |
Sign(x-axis value) ≠ Sign(y-axis value)

**Fig. S5. Kinetics of PiSCES signatures for agonist and antagonist stimuli in LC13ab.huCD8ab.JRT3 cells.** PiSCES signatures of LC13ab.huCD8ab.JRT3 cells stimulated for **(A-D)** 10 seconds, **(E-H)** 1 minute, **(I-L)** 5 minutes, or **(M-P)** 15 minutes with **(A,E,I,M)** agonist peptide, FLRGRAYGL ("RAY"; mean-log2 fold-change, RAY/no-peptide conditions; dotted lines indicate trend of non-significant protein pairs), or **(B,F,J,N)** antagonist peptide, FLRGRFYGL ("RFY"; mean-log2 fold-change, RFY/no-peptide conditions). **(C,G,K,O)** PiSCES signatures when response to RAY is directly normalized to the response to RFY (mean-log2 fold-change, RAY/RFY conditions). **(D,H,L,P)** Comparisons of mean-log2 fold-changes in abundance of protein pair hits induced by RAY versus RFY. A separate trajectory of orange points ($|x$-axis value$| > |y$-axis value$|$) that would clearly indicate antagonist-specific protein complexes is not observed.

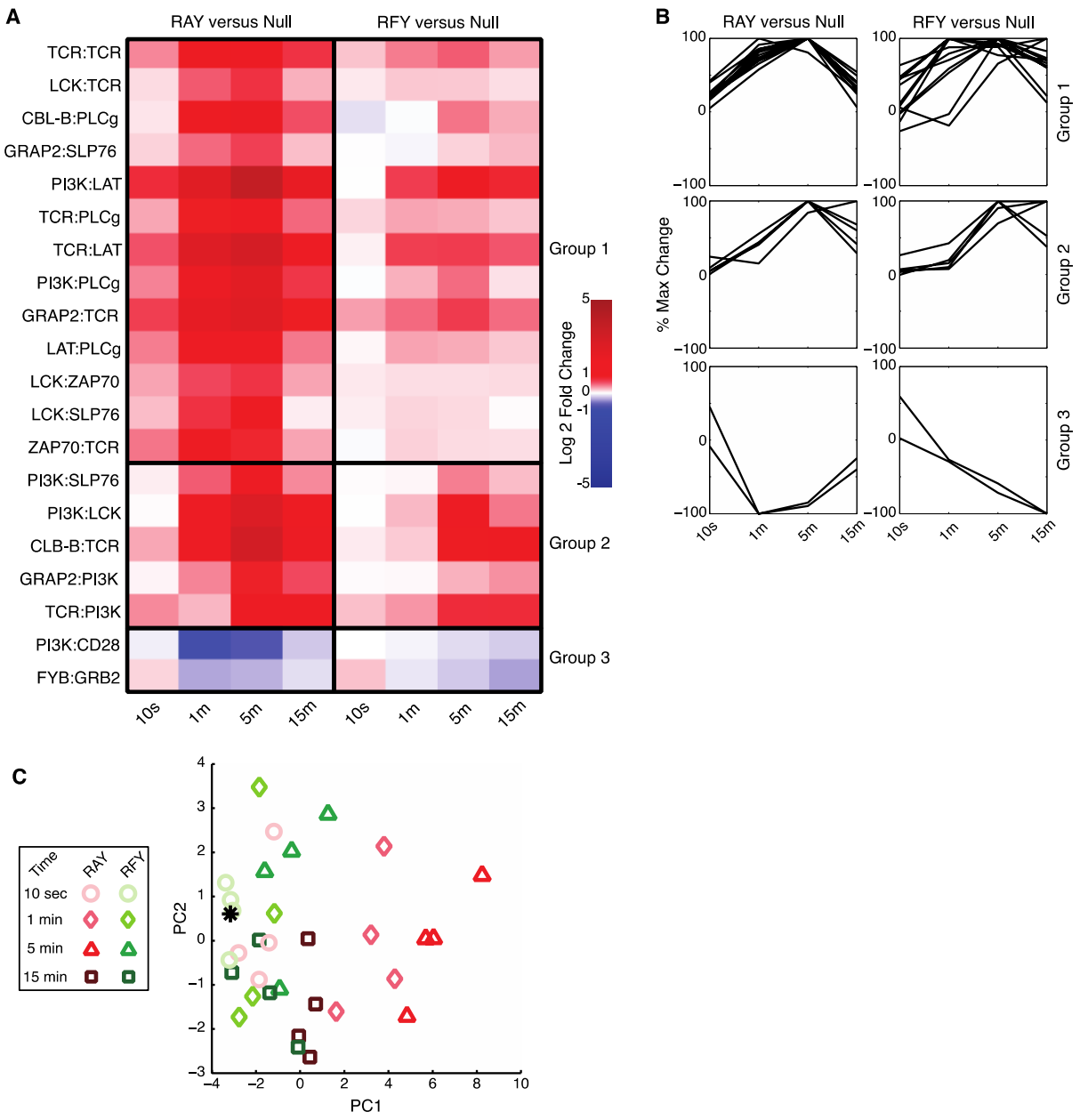


**Fig. S6. Clustering analysis for top hits observed across the kinetic for agonist versus antagonist stimuli in LC13ab.huCD8ab.JRT3 cells. (A)** K-means clustering was performed using percent-maximum log2 fold changes to define three kinetic patterns observed among the top 20 hits in response to RAY stimulation, categorized in groups 1-3. A kinetic heat map of the log2 fold changes is shown for these hits defined by the RAY stimulation condition. The

matching data points in response to RFY stimulation were seen to display similar kinetic behavior, but lower intensity fold-changes than those induced by RAY stimulation. **(B)** K-means clustering data displayed as percent-maximum log2 fold change shows that the three kinetic behavior groups defined by response to RAY stimulation (left) also described the overall kinetic behavior of the same protein pairs in response to RFY stimulation (right). **(C)** With experimental n = 4 per time point, data across 10 seconds, and 1-, 5-, and 15-minute time points were used to generate a kinetic PCA matrix. Subjectively, it appears that data for response to RAY versus RFY are distinguishable but relatively close to each other at each time point, with the time point of stimulation playing a major role in data placement in 3D analysis space, and RAY data appearing farther than RFY data from a zero-stimulation point (*).

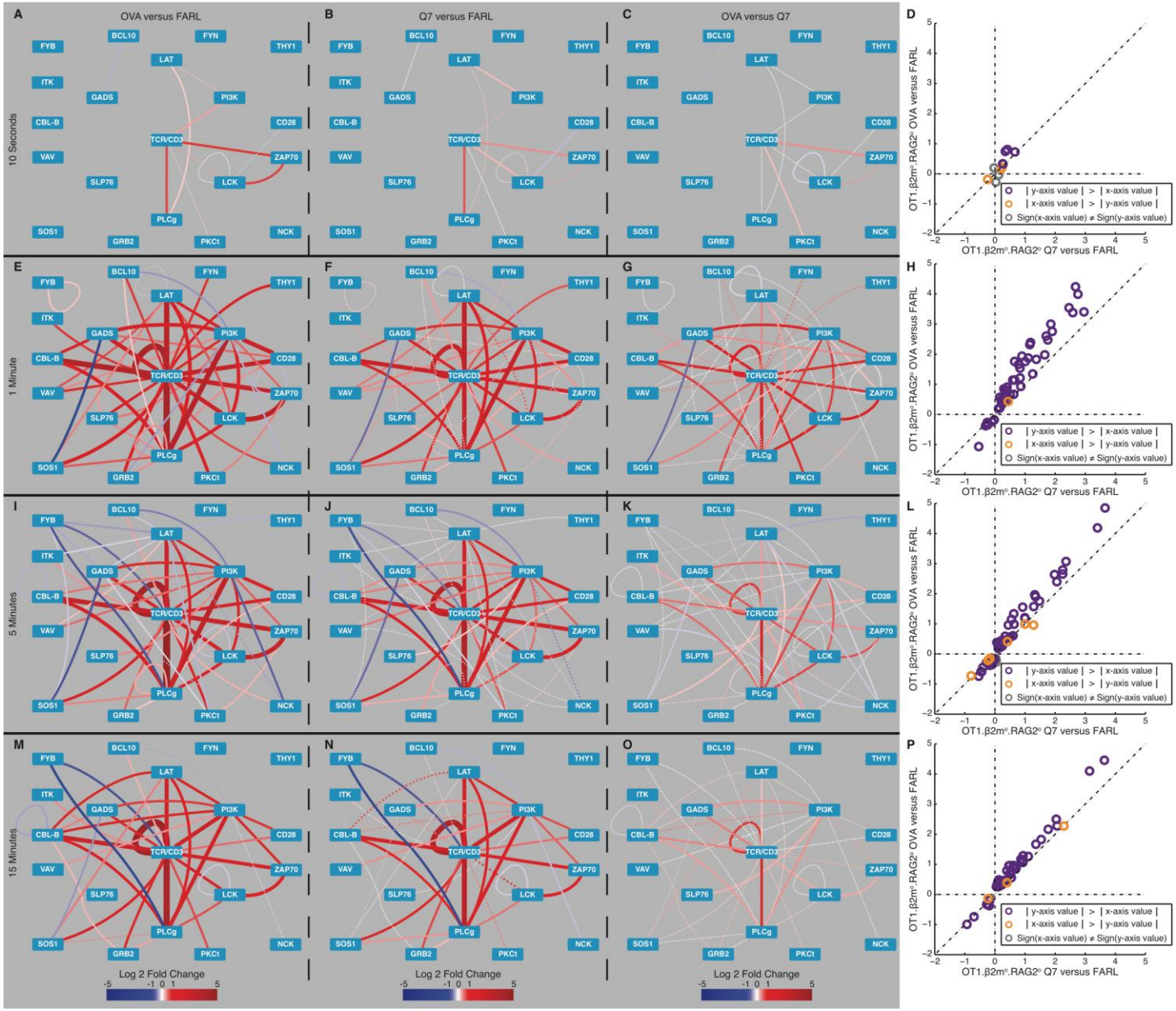
A
OVA versus FARL
B
Q7 versus FARL
C
OVA versus Q7
D
10 Seconds
1 Minute
5 Minutes
15 Minutes
E
F
G
H
I
J
K
L
M
N
O
P
BCL10
FYN
THY1
FYB
LAT
ITK
GADS
PI3K
CBL-B
CD28
TCR/CD3
VAV
ZAP70
SLP76
LCK
PLCg
SOS1
GRB2
PKCt
NCK
Log 2 Fold Change
-5 -1 0 1 5
OT1.β2m°.RAG2° OVA versus FARL
OT1.β2m°.RAG2° Q7 versus FARL
| y-axis value | > | x-axis value |
| x-axis value | > | y-axis value |
Sign(x-axis value) ≠ Sign(y-axis value)

**Fig. S7. Kinetics of PiSCES signatures for agonist and antagonist stimuli in OT1ab.muCD8ab.JRT3 cells.** PiSCES signatures of OT1ab.muCD8ab.JRT3 cells stimulated for **(A-D)** 10 seconds, **(E-H)** 1 minute, **(I-L)** 5 minutes, or **(M-P)** 15 minutes with **(A,E,I,M)** OVA peptide (mean-log2 fold-change, OVA/FARL conditions; dotted lines indicate trend of non-significant protein pairs), or **(B,F,J,N)** Q7 peptide, (mean-log2 fold-change, Q7/FARL conditions). **(C,G,K,O)** PiSCES signatures when response to OVA is directly normalized to the response to Q7 (mean-log2 fold-change, OVA/Q7 conditions). **(D,H,L,P)** Comparisons of mean-log2 fold-changes in abundance of protein pair hits induced by OVA versus Q7. A separate trajectory of orange points ($|x$-axis value$| > |y$-axis value$|$) that would clearly indicate Q7-specific protein complexes is not observed.

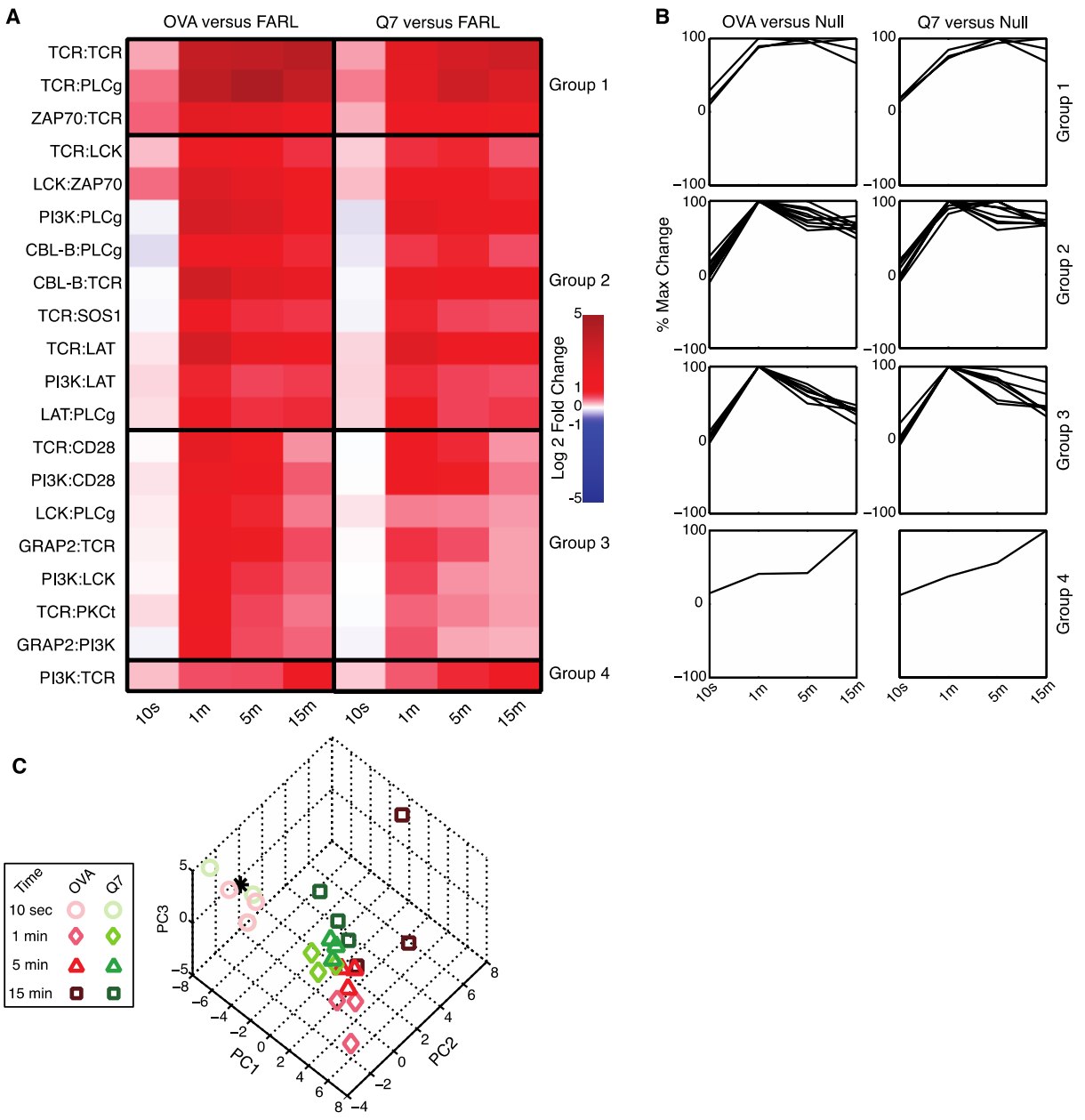


**Fig. S8. Clustering analysis for top hits observed across the kinetic for OVA versus Q7 stimuli in OT1ab.muCD8ab.JRT3 cells. (A)** K-means clustering was performed using percent-maximum log2 fold changes to define three kinetic patterns observed among the top 20 hits in response to OVA stimulation, categorized in groups 1-3. The matching data points in response to Q7 stimulation were observed to display similar kinetic behavior, but lower intensity fold-

changes than those induced by OVA stimulation. **(B)** K-means clustering data displayed as percent-maximum log2 fold change shows that the three kinetic behavior groups defined by response to OVA stimulation (left) also described the overall kinetic behavior of the same protein pairs in response to Q7 stimulation (right). **(C)** With experimental n = 4 per time point, data across 10 seconds, and 1-, 5-, and 15-minute time points were used to generate a kinetic PCA matrix. Subjectively, it appears that data for response to OVA versus Q7 are distinguishable but relatively close to each other at each time point, with the time point of stimulation playing a major role in data placement in 3D space, and OVA data appearing farther than Q7 data from a zero-stimulation point (*).

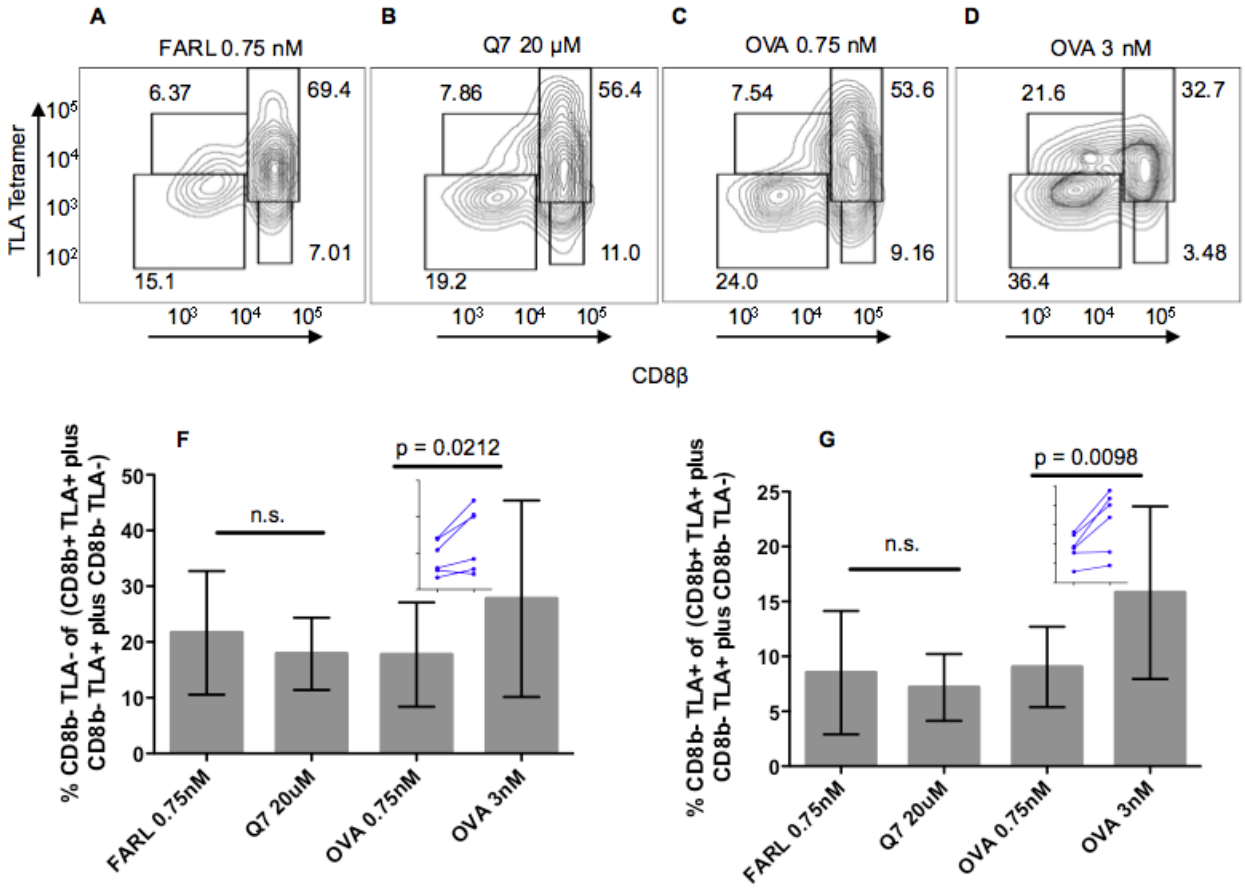


**Fig. S9. Assessment of CD8β and CD8αα (TLA+) expression in OT1.RAG2$^0$.β2m$^0$ FTOC cells.** FTOC was performed as described in Figure 4. Afterwards, flow cytometry was performed gating on live Thy1.2+ cells to assess anti-CD8β and TLA-tetramer co-staining patterns. Exogenous peptide conditions during FTOC were as follows:(**A**) FARL, 0.75 nM; **(B)** Q7, 20 μM; **(C)** OVA, 0.75 nM; **(D)** OVA, 3 nM. (**F-G**) Statistical analysis was performed to determine if OVA 3nM would induce an increase in either of the possible product subsets that would be predicted when using physiologic CD8αα SP T cell selection as a model. Data are paired within the comparisons that assess statistical significance, with data pairs shown (blue, inset) for statistically significant differences. **(F)** Relative frequency of CD8β- TLA- cells as a percentage of CD8β+ TLA+ *plus* CD8β- TLA- *plus* CD8β- TLA+ cells. **(G)** Relative frequency of CD8β-

TLA+ cells as a percentage of CD8β+ TLA+ *plus* CD8β- TLA- *plus* CD8β- TLA+ cells. Data from one of two independent experiments are shown (A-D), with both experiments included in summary data and statistics (E-F). Paired data analysis was part of the experimental design, since the two lobes of each fetal thymus was split between either FARL and Q7 conditions, or OVA 0.75 nM and OVA 3 nM conditions. Statistical significance was determined using paired Student's t-test, one-tailed, $P < 0.05$.

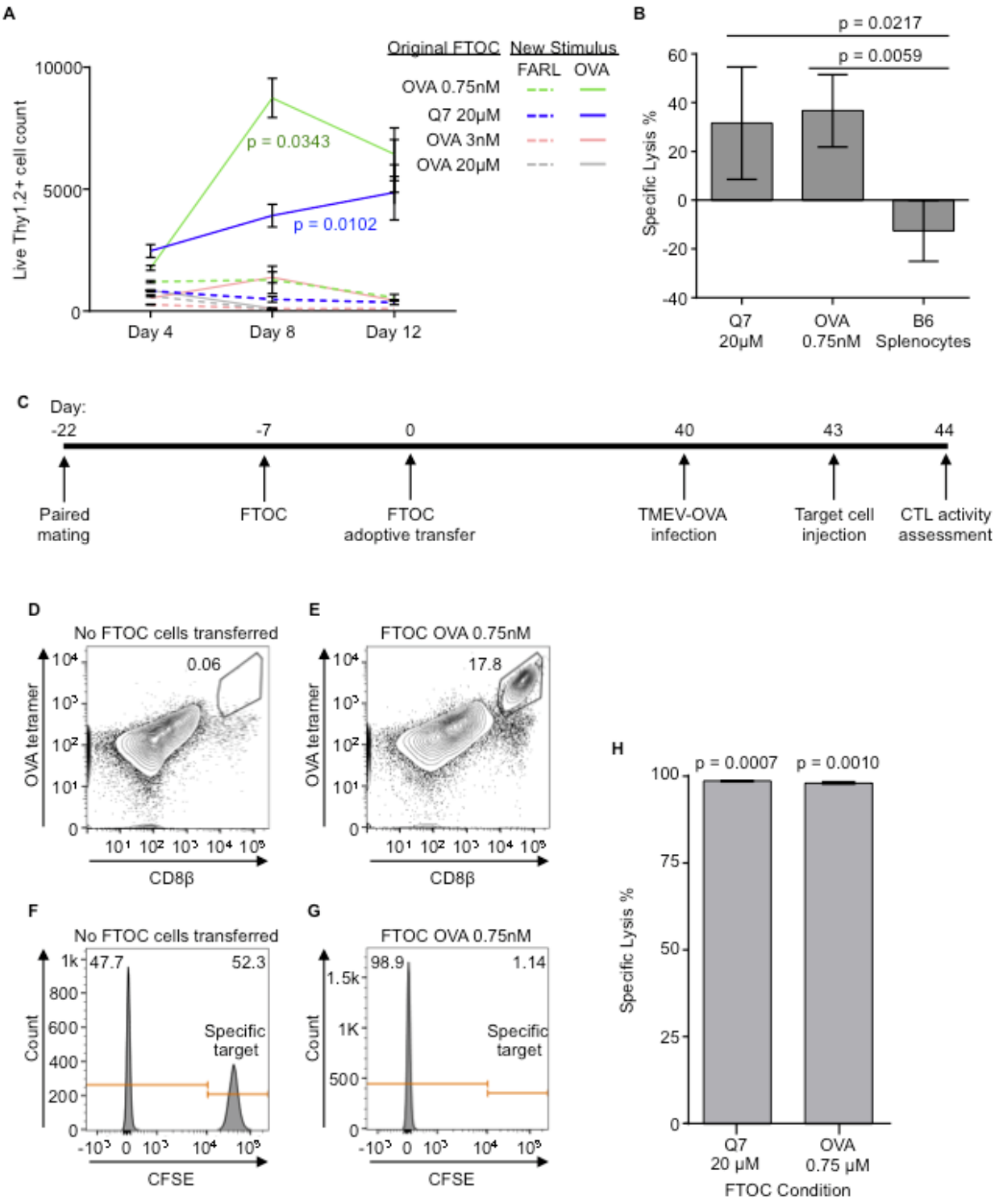


**Fig. S10. FTOCs from positive selection conditions can be induced by antigenic stimulation to proliferate and kill target cells.** FTOC was performed as described in Figure 4, after which cells were harvested and mixed with CD3$\varepsilon^0\zeta^0$splenocyte APCs that had been previously pulsed

with 10 nM FARL or OVA peptides.After 3 days of co-culture, exogenous mouse IL-2 was added and incubation continued up to 12 total days, post-FTOC. **(A)** Live Thy1.2+ T cell counts were obtained on the days indicated, post-co-culture. T cell expansion occurred when cells from either of the two FTOC conditions favoring positive selection (Q7 20 μM or OVA 0.75 nM) was subsequently stimulated by OVA-bearing APCs. Statistically significant p-values are reported to determine if T cell counts were higher in the New Stimulus OVA versus FARL conditions; Student's t-test, one-tailed, $P < 0.05$. **(B)** On day 12 post-co-culture, CTL potential of positive selection FTOC-generated cells was assessed using a new set of CD3$\varepsilon^0\zeta^0$splenocyte APCs as targets, this time loaded with 10 μM FARL or OVA peptides. Specific lysis was calculated, showing that both Q7-generated and OVA 0.75nM-generated T cells possessed specific cytotoxic activity when compared to B6 splenocytes. Statistical significance was determined using Student's t-test, one-tailed, $P < 0.05$. **(C-H)** Single-cell suspensions from FTOCs favoring positive selection were adoptively transferred into $Rag2^0.IL2Rg^0$ mice. After 40 days, mice were infected by i.p. injection of TMEV-OVA, which was followed 3 days later by i.v. injection of Ly5.1+ congenic splenocyte APCs that were composed of an equal mixture of FARL-loaded (CFSE-low) and OVA-loaded (CFSE-high) cells. One day later, host splenocytes were harvested and subjected to flow cytometry to assess the extent to which killing of specific OVA-bearing target cells occurred. **(C)** Timeline of the experimental procedure. **(D-H)** Data from the final day of harvest, day 44.**(D)** Negative control $Rag2^0.IL2Rg^0$ mice that received no FTOC cells by adoptive transfer had virtually no cells that stained double-positive with anti-CD8β and H-2Kb/SIINFEKL (OVA)-tetramer. **(E)** Adoptive transfer of FTOC cells from OVA 0.75 nM condition into $Rag2^0.IL2Rg^0$ mice supplied CD8β+ OVA-tetramer+ cells. **(F)** Spleens harvested from $Rag2^0.IL2Rg^0$ mice that received no FTOC cells had almost equal numbers of FARL-

loaded (CFSE-low) and OVA-loaded (CFSE-high) APCs. **(G)** $Rag2^0.IL2Rg^0$ recipients of adoptive transfers from the 0.75 nM FTOC condition had spleens with FARL-loaded (CFSE-low) APCs, but very few OVA-loaded (CFSE-high) APCs. **(H)** Specific target killing from recipient mice that had received FTOC cells from conditions of Q7 20 μM or OVA 0.75 nM was statistically higher than the specific killing observed in mice that received no adoptive transfer. Statistical significance was determined by Student's t-test, one-tailed, with ≥2recipient mice per condition.Representative data from one of two independent experiments are shown.

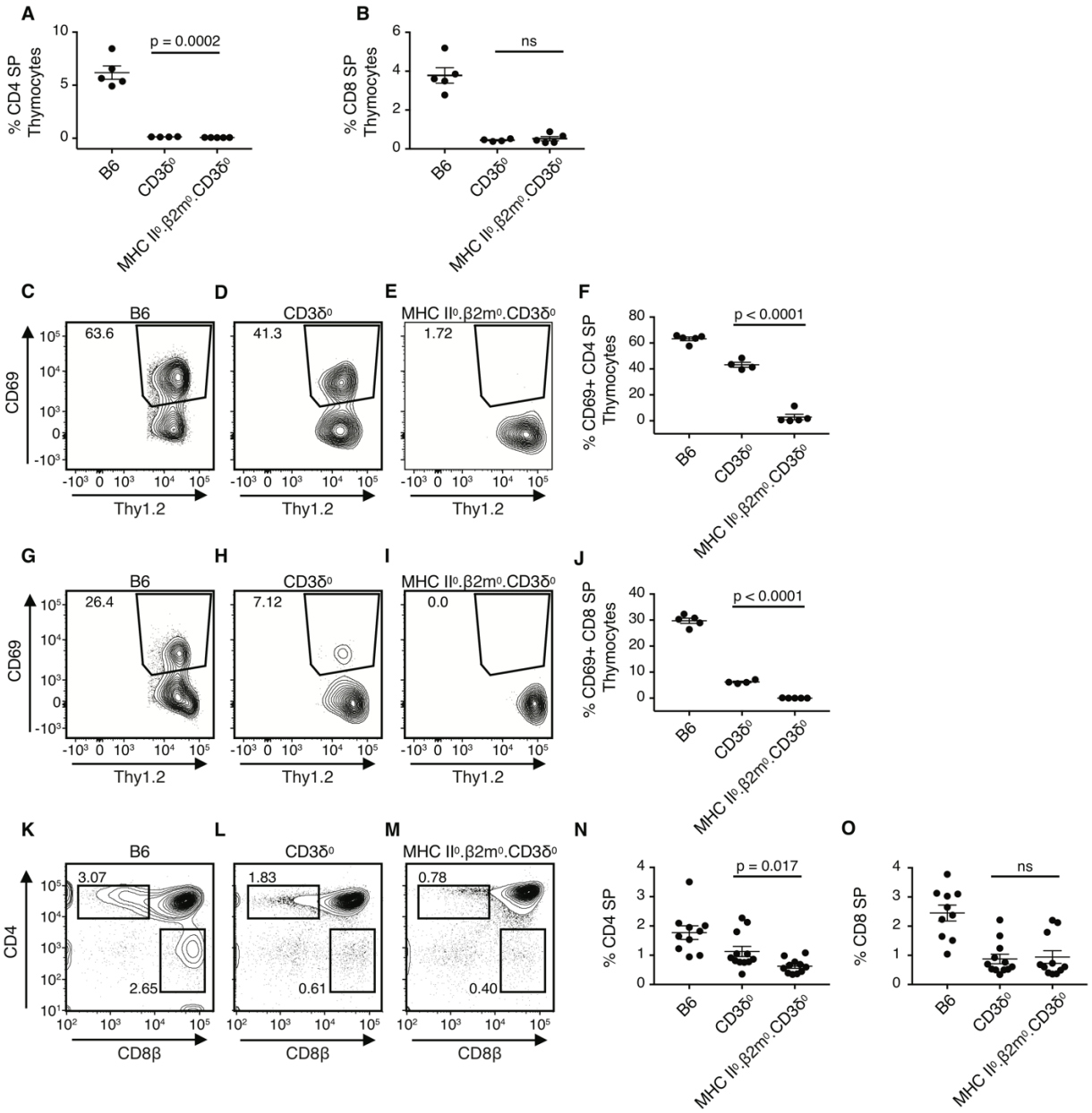


**Fig. S11. MHC-dependent signaling generates residual αβ T cells in CD3δ$^0$ mice.** By performing flow cytometry on single cell suspensions of juvenile thymocytes and gating on live Thy1.2+ cells, percentages from the indicated genotypes were calculated for **(A)** CD4 SP thymocytes, and **(B)** CD8 SP thymocytes. The percentage of CD4 SP thymocytes that were Thy1.2+ and CD69+ was obtained for the same genotypes **(C-E)**, with **(F)** data from multiple mice summarized. Likewise, the percentage of CD8 SP thymocytes that were Thy1.2+ and

CD69+ was obtained for the genotypes **(G-I)**, with **(J)** data from multiple mice summarized. Flow cytometry assessments were made for thymocytes in FTOC from the same three genotypes **(K-M)**, and the percentage was calculated of **(N)** CD4 SP cells, and **(O)** CD8 SP cells. For juvenile thymi, mouse n was $\geq 4$ per genotype, while for FTOC each selection condition was performed with $n \geq 10$ for each genotype. Two-tailed, unpaired t-test was used to determine statistical significance, $P < 0.05$.

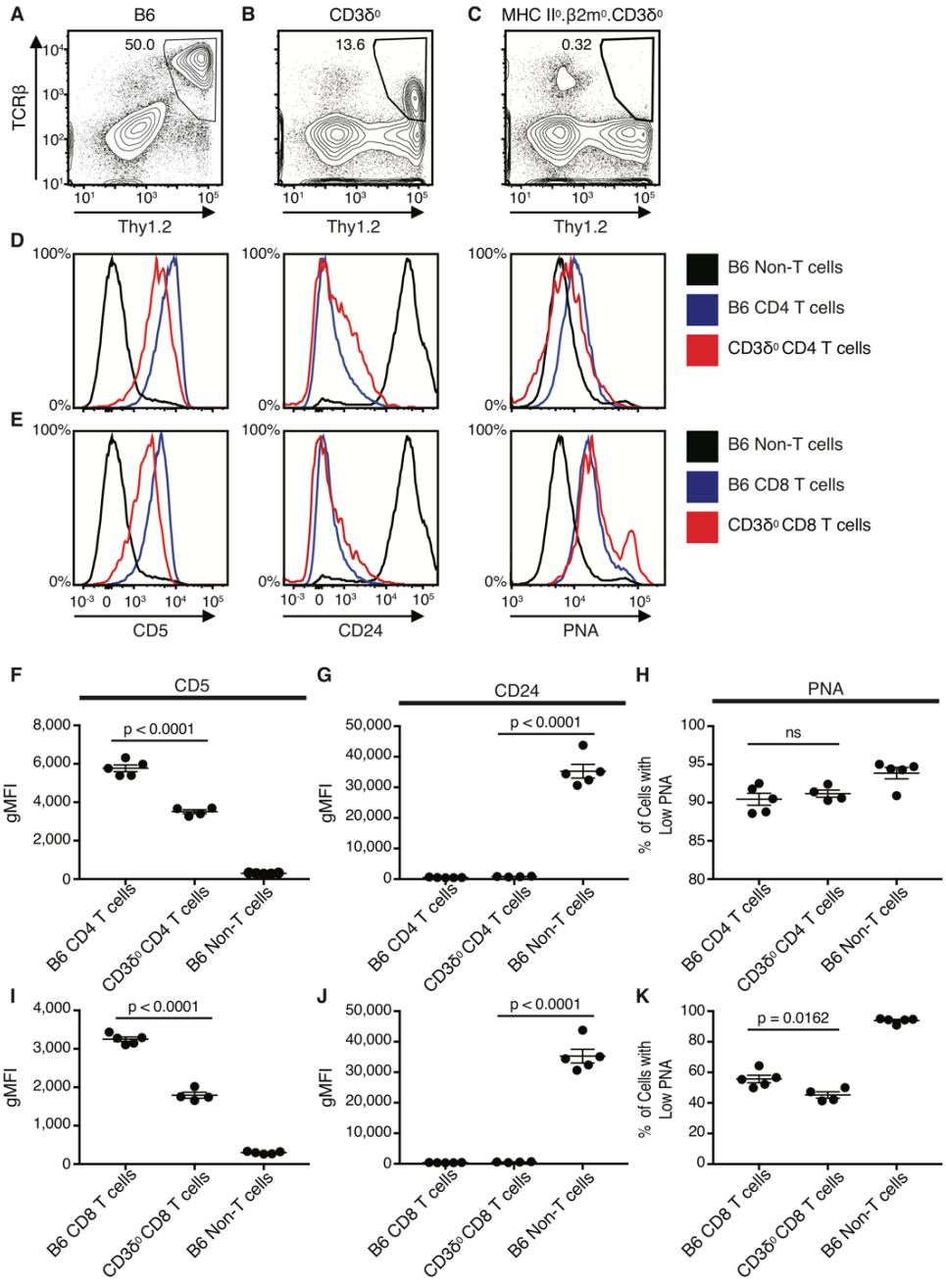


**Fig. S12. Developmental and maturation markers on peripheral T cells of wild-type and mutant mice.** Live splenic lymphocytes were gated on CD4 or CD8 co-receptors (CD4 in A-C), and further gated on Thy1.2+ TCRβ+ surface expression from mice from genotypes **(A)** wild-type B6, **(B)** CD3δ$^0$, and **(C)** MHC II$^0$.β2m$^0$.CD3δ$^0$. Note that peripheral T cells from B6 mice expressed high surface TCR, while CD3δ$^0$ T cells were surface TCR-low. Because there were

virtually no T cells in (C), MHC $II^0.\beta2m^0.CD3\delta^0$ is not assessed in the rest of this figure, while flow cytometry staining controls are provided by B6 splenic non-T cells (Thy1.2-negative). Surface CD5, CD24, and PNA-staining were assessed for **(D)** CD4 T cells and **(E)** CD8 T cells, and data from multiple mice is summarized for **(F-H)** CD4 T cells and **(I-K)** CD8 T cells. Mouse n was $\geq 4$ for each genotype, and unpaired, two-tailed t-test was employed to determine statistical significance, $P < 0.05$.

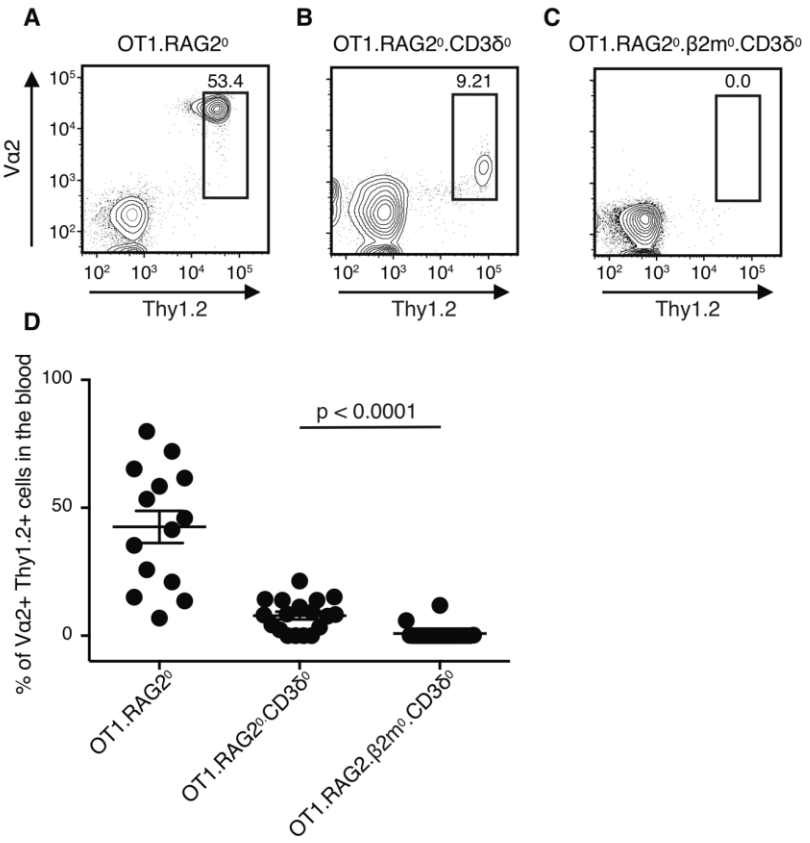


**Fig. S13. The few peripheral T cells in OT1.RAG2$^0$.CD3δ$^0$ mice require MHC class I for their generation/survival.** The relative frequency of OT1 T cells in peripheral blood was analyzed by flow cytometry detecting Vα2+ Thy1.2+ live lymphocytes. **(A)** These cells were readily detected in blood from OT1.Rag2$^0$ mice. **(B)** On average, OT1.RAG2$^0$.CD3δ$^0$mice had substantially fewer of these cells, and those that were present were confirmed CD3δ$^0$ due to lower expression of surface Vα2 TCR/CD3. **(C)** Such cells were virtually absent in blood from OT1.RAG2$^0$.β2m$^0$.CD3δ$^0$ mice, demonstrating that MHC class I was required for their generation/survival. **(D)** The difference between OT1.RAG2$^0$.CD3δ$^0$and OT1.RAG2$^0$.β2m$^0$.CD3δ$^0$ mice was statistically significant.N ≥ 14 per experimental group, two-tailed Student's t-test, P < 0.05.

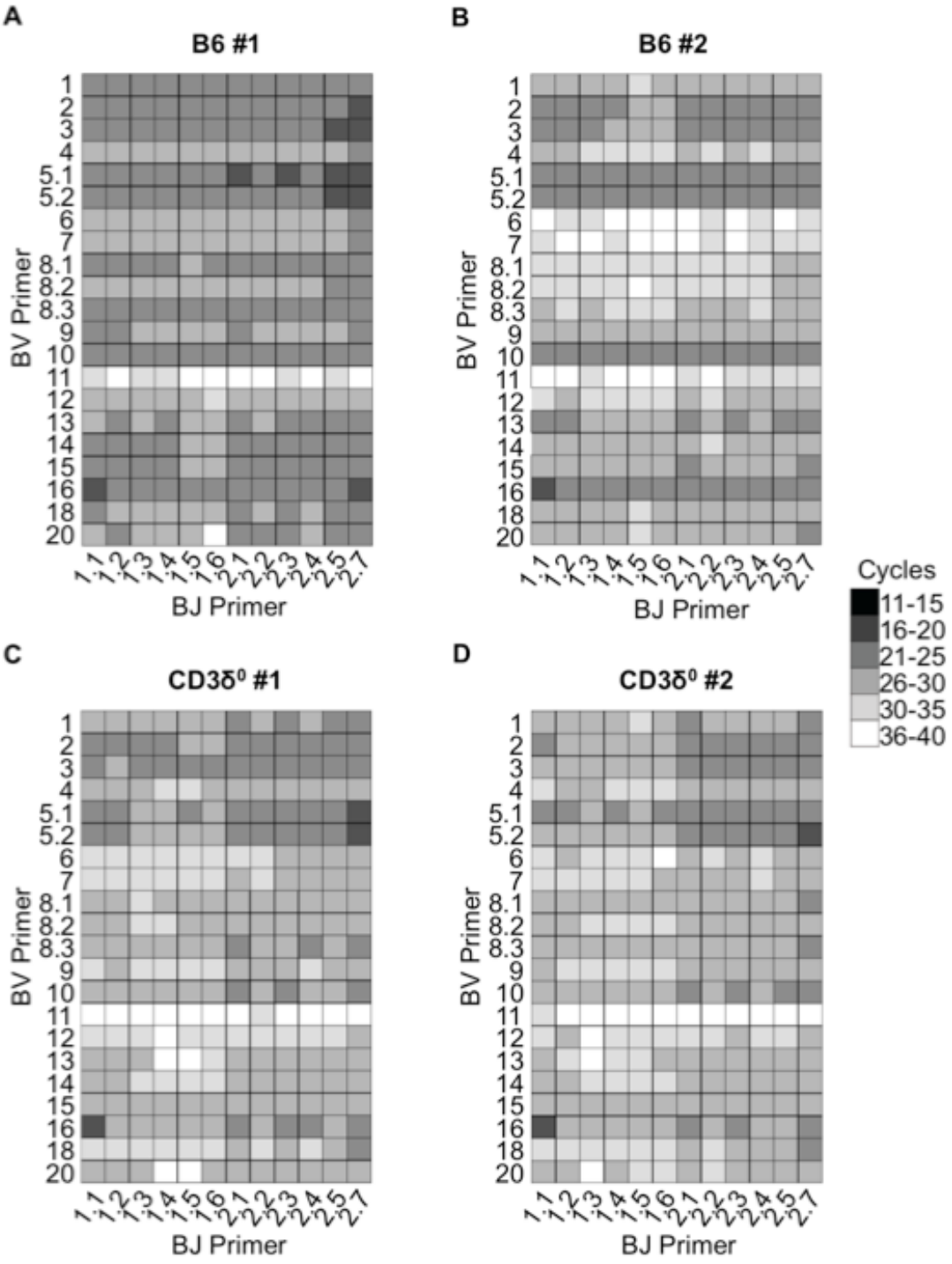


**Fig. S14. Diverse TCR repertoire in individual B6 and CD3δ$^0$ mice.** This is an alternative display of data shown in Fig. 7, but whereas Fig. 7 shows average Ct values from these two mice from each genotype, the data for each individual mouse is shown here for **(A-B)** B6, and **(C-D)** CD3δ$^0$ mice.

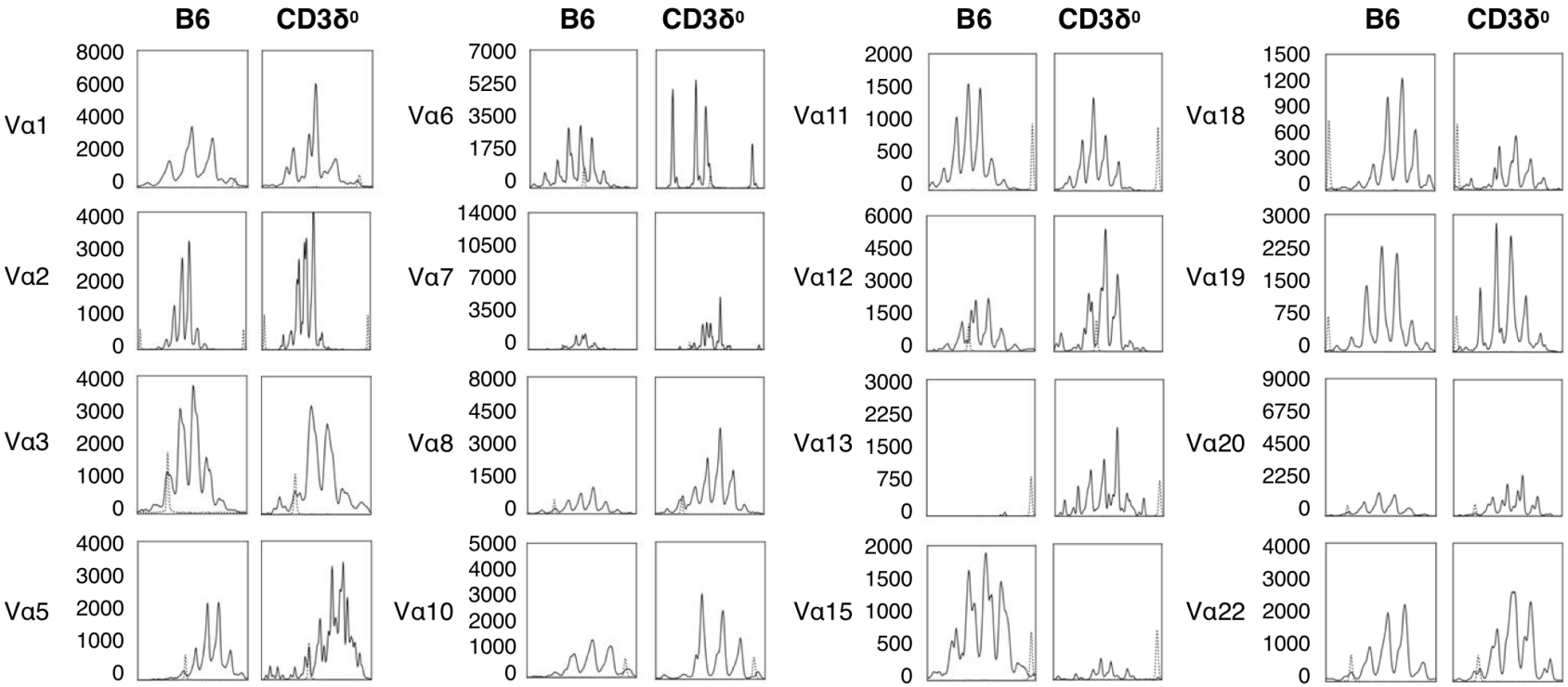


**Fig. S15. Multiple peripheral TCRα transcripts in B6 and CD3δ$^0$ mice.** TCRαspectratyping was performed across a survey of V-genes expressed in splenocytes from B6 and CD3δ$^0$ mice. Each panel displays data from a single mouse (not pooled, from two mice per genotype tested).

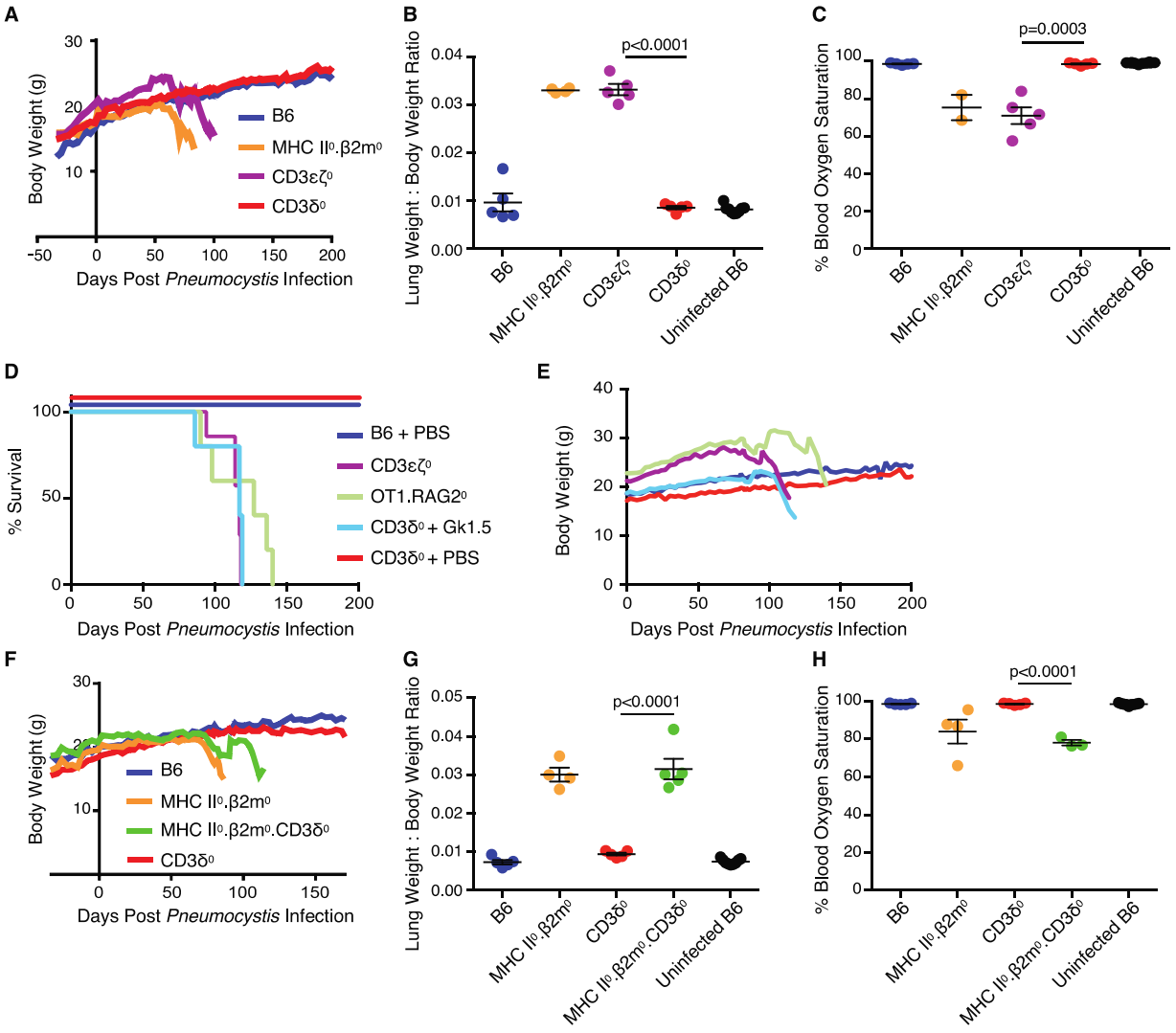


**Fig. S16. T cells in CD3δ$^0$ mice provide immune activity against PCP. (A-C)** To assess the extent of T cell immune activity in a CD3δ$^0$ setting, mice from the listed genotypes were infected with *Pneumocystis*murina. **(A)** Weight was monitored regularly throughout the experiment. **(B)** Upon sacrifice, lungs were harvested and weighed. **(C)** Just prior to sacrifice, blood oxygen saturation was measured for some of the mice. **(D-E)** To assess the extent of CD4 cell immune activity in a CD3δ$^0$ setting, mice from the listed genotypes were either depleted of CD4 cells with GK1.5 anti-CD4 mAb injections, or were given control injections of PBS as indicated, and

were infected with *Pneumocystis*murina(mouse $n \geq 5$ for all groups, except n=3 for $CD3\delta^0$+PBS). **(D)** Kaplan-Meier curves display survival defined by mice being sacrificed upon loss of 20% weight, where $CD3\delta^0$ + PBS and $CD3\delta^0$ + GK1.5 were statistically different ($P = 0.015$) by Log-Rank Mantel-Cox test. **(E)** Weight was monitored regularly throughout the experiment. **(F-H)** To test the role of MHC in mediating protection from PCP in a $CD3\delta^0$ setting, mice from the listed genotypes were infected with *Pneumocystis*murina. **(F)** Weight was monitored regularly throughout the experiment. **(G)** Upon sacrifice, lungs were harvested and weighed. **(H)** Just prior to sacrifice, blood oxygen saturation was measured for some of the mice.P-values denote statistical significance using unpaired, two-tailed Student's t-test, $P < 0.05$.

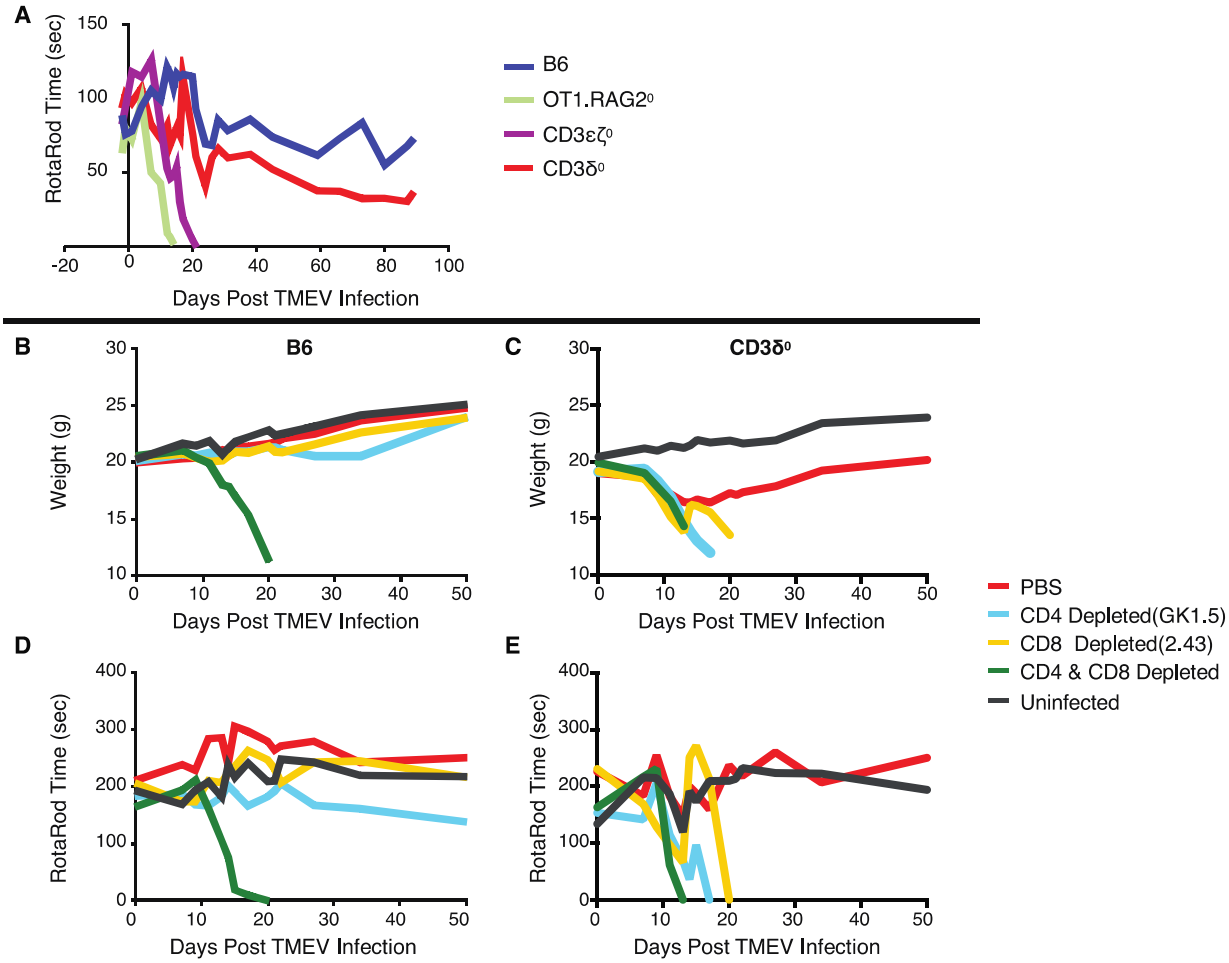


**Fig. S17. T cells in CD3δ$^0$ mice provide immune activity against TMEV. (A)** To assess the extent of T cell immune activity in a CD3δ$^0$ setting, mice from the listed genotypes were infected with TMEV (mouse n ≥ 4 for all genotypes, except n=3 for CD3ε$^0$ζ$^0$). Functional deficit was monitored frequently throughout the experiment by RotaRod performance, measured as the average time elapsed prior to falling off the apparatus in two trials. **(B-E)** To assess CD4 and CD8 T cell immune activity, B6 and CD3δ$^0$ mice were either depleted of CD4 cells with GK1.5 anti-CD4 mAb injections, depleted of CD8 cells with 2.43 anti-CD8 mAb injections, depleted of both CD4 and CD8 cells, or were PBS-control injected as indicated, and were infected with TMEV (mouse n = 4 for all groups, except n=3 for CD3δ$^0$+PBS). **(B-C)** Weight was monitored

regularly throughout the experiment. **(D-E)** Functional deficit was monitored frequently throughout the experiment by RotaRod performance, measured as the average time elapsed prior to falling off the apparatus in two trials.

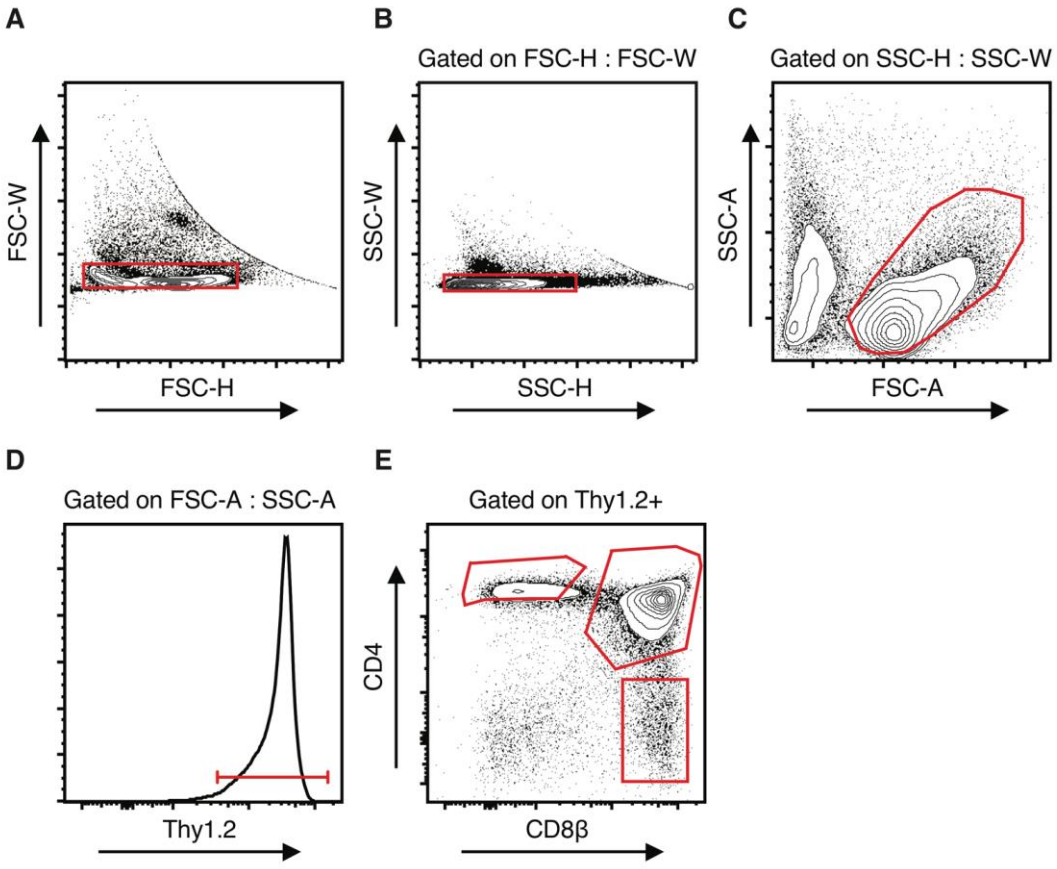


**Fig. S18. Example gating used for flow cytometry data.** The data corresponds with thymocytes from the B6 mouse shown in Fig. 5A.From left to right, doublet exclusion is invoked gating first on **(A)** FSC-H and FSC-W, followed by **(B)** SSC-H and SSC-W.Next, live lymphocytes are gated by **(C)** FSC-A and SSC-A, followed by gating on **(D)** the Thy1.2+ subset.**(E)** T-lineage cells are thus displayed as seen in Fig. 5A.

**Table S1. Validated Ab pairs used to identify each mouse protein target.** Cells used as specificity controls are listed in the right column.Where possible, if Abs cross-reacted with human homologs, target-negative Jurkat mutant cell lines were used. Otherwise, GeneAtlas RNA expression profiles were used to select a cell type that lacked the protein, and these were used as controls. For widely expressed targets, RNAi was used.

| | Target | Capture Ab | Probe Ab | Cell specificity control |
|---|---|---|---|---|
| 1a | TCR | MR9-4 (in-house) | JOVI-1 (in-house) | JRT3 (target-deficient Jurkat mutant) |
| 1b | CD3z | H146 (in-house) | 6B10 (eBioscience) | X63 (myeloma) |
| 2 | LAT | 661002 (R&D Systems) | 06-807 (Millipore) | Anj (target-deficient Jurkat mutant) |
| 3 | ZAP70 | D1C10E Cell Signaling) | 1E7 (eBioscience) | P116 (target-deficient Jurkat mutant) |
| 4 | SLP76 | H76 (Biolegend) | 06-548 (Millipore; Figs. 1-4, S2-S7), or H-300 (Santa Cruz; Fig. 6) | J-14 (target-deficient Jurkat mutant) |
| 5 | PLCg | 10/PLC (BD Biosciences) | NBP1-61254 (Novus) | Jgamma-1 (target-deficient Jurkat mutant) |
| 6 | PI3K p85 | U5 (Thermo) | AB6 (Millipore) | X63 (B cell myeloma) |
| 7 | VAV | 9C1 (Novus) | 05-219 (Millipore) | J-VAV (target-deficient Jurkat mutant) |
| 8 | LCK | 73A5 (Cell Signaling) | 3A5 (Santa Cruz) | Jcam-1 (target-deficient Jurkat mutant) |
| 9 | CD28 | E18 (Biolegend) | 37.51 (Biolegend) | Renca |
| 10 | GRB2 | 81/Grb (BD Biosciences) | SAB4501290 (Sigma) | Renca |
| 11 | SOS1 | SOS-01 (AbCam) | 07-337 (Millipore) | RNAi knockdown in Jurkat |
| 12 | NCK | Y531 (AbCam) | 06-288 (Millipore) | Mouse cerebellum |
| 13 | FYN | FYN59 (Biolegend) | Fyn15 (Santa Cruz) | Renca |
| 14 | FYB | 6348 (AbDSerotec) | EP25464 (AbCam) | Renca |
| 15 | ITK | Y402 (AbCam) | 2F12 (BD Biosciences) | Renca |
| 16 | GADS | UW40 (Novus) | 1G12 (AbNova) | Renca |
| 17 | Cbl-b | 246C5A (AbCam) | B-5 (Santa Cruz) | NIH3T3 |
| 18 | BCL10 | EPR3174 (AbCam) | 4F8 (Thermo) | NIH3T3 |
| 19 | PKC-theta | MAB4368 (R&D Systems) | NBP1-00985 (Novus) | X63 (B cell myeloma) |
| 20 | Thy1 | 30-H12 (eBioscience) | 53-2.1 (BD Biosciences) | X63 (B cell myeloma) |